

# 1 Aerosol optical properties derived from POLDER- 2 3/PARASOL (2005-2013) over the western Mediterranean Sea 3 – Part 2 : Spatial distribution and temporal variability

4  
5 Isabelle Chiapello<sup>1</sup>, Paola Formenti<sup>2</sup>, Lydie Mbemba Kabuiku<sup>2</sup>, Fabrice Ducos<sup>1</sup>, Didier  
6 Tanré<sup>1</sup>, François Dulac<sup>3</sup>

7  
8 <sup>1</sup>Univ. Lille, CNRS, UMR 8518 – LOA – Laboratoire d’Optique Atmosphérique, F-59000 Lille, France

9 <sup>2</sup>LISA, CNRS UMR 7583, Université Paris Est Créteil, Université de Paris, IPSL, Créteil, France

10 <sup>3</sup>LSCE/IPSL, CEA-CNRS-UVSQ, Université Paris-Saclay, Gif-sur-Yvette, France

11  
12 *Correspondence to:* Isabelle Chiapello (isabelle.chiapello@univ-lille.fr)

13  
14  
15 **Abstract.** The Mediterranean atmosphere is impacted by a variety of natural and anthropogenic aerosols, which  
16 exert a complex and variable pressure on the regional climate and air quality. This study focuses on the western  
17 Mediterranean Sea (west of longitude 20°E) using the full POLDER-3/PARASOL aerosol data record derived  
18 from the operational clear-sky ocean algorithm (collection 3) available from March 2005 to October 2013. This  
19 8.5-yr satellite data set includes retrievals at 865 nm of the total, fine, and coarse mode aerosol optical depth (AOD,  
20 AOD<sub>F</sub>, and AOD<sub>C</sub>, respectively), Angström exponent (AE), and the spherical/non-spherical partition of the coarse-  
21 mode AOD (AOD<sub>CS</sub> and AOD<sub>CNS</sub>, respectively), that have been carefully validated over the study region (Formenti  
22 et al., 2018). Here we analyze the spatial distribution, the seasonal cycle, and interannual variability of this  
23 ensemble of advanced aerosol products in three latitude bands (34-38°N, 38-42°N, and >42°N) and for three sites  
24 (Ersa, Barcelona, Lampedusa) distributed on the western basin. POLDER-3 retrieves the high influence of north  
25 African desert dust over the region, which largely controls the spatial distributions (south-to-north decreasing  
26 gradient) and seasonal cycles (spring/summer maximum) of both AOD and coarse AOD, including its non-  
27 spherical component. In contrast, the coarse spherical component of AOD remains relatively homogeneously low  
28 all year long over the region, whereas fine mode AOD are generally more elevated in the eastern part of the region  
29 of study, especially north of the Adriatic Sea. From 2005 to 2013, annual POLDER-3 AOD evolution shows a  
30 decreasing trend of 0.0030 per year in absolute value at 865 nm (0.0060 per year at 550 nm). Such a downward  
31 evolution is much more pronounced and spatially extended for AOD<sub>F</sub> (- 0.0020 per year at 865 nm) than for AOD<sub>C</sub>.  
32 Our analysis also suggests that the North Atlantic Oscillation (NAO) index explains a significant part of the  
33 interannual variability of POLDER-3 AOD<sub>C</sub>, reflecting its role on the frequency of Saharan dust transport over the  
34 region. Finally, the POLDER-3 dataset highlights an improvement of air quality related to the fine aerosol  
35 component, with a marked evolution toward more frequent occurrence of clean conditions ( $\geq 75\%$  of daily AOD<sub>F-  
36 865 nm</sub> < 0.05) at the end of the period of study (2010-2013) over most of the western Mediterranean Sea, and much  
37 less evidence of such a large-scale evolution for the coarse fraction. Therefore, despite the high and variable  
38 influence of mostly natural north African dust over the region, the POLDER-3 advanced aerosol dataset appears  
39 sufficiently accurate to successfully resolve the concurrent downward trend of fine, primarily anthropogenic  
40 particles, most likely related to reduced emissions in the surrounding European countries.

41

## 42 1 Introduction

43  
44 Due to the contributions of diverse natural and anthropogenic sources and because of their relatively short lifetime  
45 in the troposphere, aerosols consist in a complex, timely and spatially variable mixture of particles (Boucher,  
46 2015). As aerosol impacts, especially in terms of air quality degradation and radiative forcing contribution to  
47 climate change, strongly depend on both very variable aerosol loads and properties, they require a dedicated  
48 reliable monitoring. Despite a number of measurements efforts deployed in the last decades (Laj et al., 2009;  
49 Pandolfi et al., 2018; Formenti, 2020; Laj et al., 2020), the variety of atmospheric particles, in terms of loads, size  
50 ranges, shapes, chemical compositions, and optical properties remains partially characterized. Indeed, the  
51 monitoring of the spatial, temporal, and vertical variability of all these physico-chemical parameters in both an  
52 accurate and comprehensive way is still a challenge. Significant advances have been achieved by intensive field  
53 experiments deploying detailed but limited in time and space *in situ* measurements of aerosol chemical, physical,  
54 and optical properties (e.g. Denjean et al., 2016; Di Biagio et al., 2016). In parallel, remote sensing observations,  
55 especially those from ground-based global aerosol networks, like AERONET (Holben et al., 2001), and dedicated  
56 advanced aerosol satellite sensors, like MODIS (MODerate resolution Imaging Spectrometer) or POLDER  
57 (POLarization and Directionality of the Earth's Reflectances) (Tanré et al., 2011; Bréon et al., 2011; Remer et al.,  
58 2020), have made considerable progress in expanding in time and space the aerosol datasets acquired from field-  
59 experiments. Thus, remote sensing has become an essential complementary tool, able to provide unique repetitive  
60 and large-scale view of aerosol loads and properties evolution. The combination of both types of measurements,  
61 i.e. detailed *in situ* aerosol characterization and long-term repetitive aerosol properties monitored by space-borne  
62 sensors is required to improve current understanding of their evolution in terms of loads and properties and to  
63 reduce uncertainties on their impacts.

64 This paper is dedicated to a regional aerosol analysis based on retrievals from POLDER-3/PARASOL  
65 (Polarization & Anisotropy of Reflectances for Atmospheric Sciences coupled with Observations from a Lidar)  
66 satellite sensor over the period 2005-2013 in the western Mediterranean Sea. This region, impacted by  
67 demographic pressure and air quality degradation, is under the influence of both anthropogenic and natural  
68 aerosols, emitted from different types of continental and marine sources (e.g. Lelieveld et al., 2002; Di Biagio et  
69 al., 2015; Ancellet et al., 2016; Chazette et al., 2016, Claeys et al., 2017; Michoud et al., 2017; Chazette et al.,  
70 2019). Therefore, in the recent years, it has experienced an increasing scientific interest as shown by a number of  
71 studies dedicated to Mediterranean aerosol characterization through large-scale field-experiments (e.g., Di Biagio  
72 et al., 2015; Mallet et al., 2016; Ricaud et al., 2018 and references therein), modeling efforts (Rea et al., 2015;  
73 Menut et al., 2016, Sič et al., 2016; Chrit et al., 2018; Drugé et al., 2019), and satellite observations analysis (Nabat  
74 et al., 2013; Floutsi et al., 2016).

75 Previous studies relying on daily, large-scale satellite aerosol observations (Dulac et al., 1992; Moulin et al., 1998;  
76 Antoine and Nobileau 2006; Gkikas et al., 2013, 2016) have highlighted that the Mediterranean atmosphere is  
77 highly influenced by the sporadic transport of north African dust. This export causes a south to north decreasing  
78 gradient of aerosol loads, and a seasonal east-west shift characterized by a later (summer) maximum for the western  
79 basin (Moulin et al., 1998; Floutsi et al., 2016). In addition, several long-term satellite data sets have revealed the  
80 large-scale control of the North Atlantic Oscillation on the inter-annual variability of retrieved aerosol loads, in  
81 relation to this highly variable transport of dust over the region (Moulin et al., 1998; Antoine et Nobileau, 2006).  
82 Floutsi et al., (2016) climatology, based on 12 years of MODIS aerosol observations (2002-2014), has highlighted

83 a decreasing trend of aerosol loads over the Mediterranean basin. Their MODIS data set, by showing a higher  
84 decreasing trend of fine-mode aerosol loads than that of the coarse fraction, strongly suggests a lowering of  
85 anthropogenic pollution particles influence over the region, most likely related to reduced human-related  
86 emissions. In agreement with other multiyear satellite studies (Gkikas et al., 2013), Floutsi et al. (2016) also assume  
87 a certain level of decrease of the transported desert dust particles, mainly over the western sub-basin.  
88 Most of the satellite studies dedicated to interpretation of aerosol spatial and temporal variability over the  
89 Mediterranean region have been relying on MODIS retrievals (Barnaba and Gobi, 2004; Hatzianastassiou et al.,  
90 2009; Georgoulias et al., 2016), with some of them focusing of the eastern sub-basin (Georgoulias et al., 2016;  
91 Shaheen et al., 2020). Considering the complexity of the aerosol influences in the Mediterranean atmosphere and  
92 inherent uncertainties related to long-term satellite aerosol retrievals, our study aims to provide a first interpretation  
93 of an independent advanced aerosol satellite data set. For this purpose, we investigate the POLDER-3/PARASOL  
94 data set (Herman et al., 2005; Tanré et al., 2011), which offers the capacity for daily monitoring of the size-resolved  
95 aerosol properties over sea surfaces over its almost 9 years period of operation (Formenti et al., 2018).  
96 At a global scale, a careful validation of POLDER-3 aerosol retrievals has been performed for derived total and  
97 fine aerosol optical depth (AOD), through statistical comparison to coincident sun/sky photometer data of the  
98 AERONET network (Bréon et al., 2011). In a first dedicated paper (part 1 of the present paper: Formenti et al.,  
99 2018), we lead a regional comprehensive quality assessment of POLDER-3 derived aerosol parameters over the  
100 western Mediterranean Sea, based on both aerosol measurements from 17 ground-based coastal and insular  
101 AERONET sites over the period 2005-2013, and in situ airborne observations available during summer 2012 and  
102 2013 Chemistry-Aerosol Mediterranean Experiment (ChArMEx) experiments (Di Biagio et al., 2015; Mallet et  
103 al., 2016). Our analysis has highlighted quality and robustness of POLDER-3 operational aerosol retrievals over  
104 oceans, especially total, fine, and coarse AOD ( $AOD$ ,  $AOD_F$ , and  $AOD_C$ ) at 865 nm, Angström Exponent (AE),  
105 and the spherical and non-spherical partition of coarse-mode AOD ( $AOD_{CS}$  and  $AOD_{CNS}$ ) over this region. In this  
106 paper, the advanced aerosol data set provided by POLDER-3 over its operating period, i.e. from March 2005 to  
107 October 2013, is investigated in terms of spatial variability and temporal evolution of aerosol load, size, and shape  
108 properties over the western Mediterranean Sea.

109

## 110 **2 POLDER-3 instrument and derived aerosol operational products over ocean**

111

112 POLDER-3 (POLarization and Directionality of the Earth's Reflectances) instrument on board the PARASOL  
113 (Polarization & Anisotropy of Reflectances for Atmospheric Sciences coupled with Observations from a Lidar)  
114 mission is dedicated to advanced aerosol monitoring (Tanré et al., 2011). PARASOL, launched in December 2004  
115 in order to be part of the A-Train, has been in operation from March 4, 2005 to October 10, 2013. Over this period,  
116 data availability is 91%. The explanations for the 9% loss of data are multiple: orbital maneuvers, instrument put  
117 on standby for security reasons, data transmission between the payload and the receiving station, and problems  
118 encountered with the stellar sensor. POLDER-3 payload consisted of a digital camera with a 274 x 242 –pixel  
119 CDD detector array, wide-field telecentric optics and a rotating filter wheel enabling measurements in 9 spectral  
120 channels from blue (443 nm) to near-infrared (1020 nm). Polarization measurements were performed at 490 nm,  
121 670 nm, and 865 nm. With an acquisition of a sequence of images every 20 sec, the instrument could observe  
122 ground targets from up to 16 different angles,  $\pm 51^\circ$  along track and  $\pm 43^\circ$  across track (Tanré et al., 2011). The  
123 original pixel size is 5.3 km x 6.2 km at nadir. Algorithms have been developed to process the POLDER

124 measurements in order to retrieve aerosol parameters at  $18.5 \times 18.5 \text{ km}^2$  superpixel resolution ( $3 \times 3$  pixels). In  
125 this paper, we use the operational clear-sky ocean retrieval algorithm (Herman et al., 2005) derived from collection  
126 3, corresponding to the latest update performed in 2014 that included calibration improvements (Fougnie, 2016).  
127 This algorithm, described in details by Herman et al. (2005) and Tanré et al. (2011), has been slightly improved in  
128 collection 3 regarding non-spherical particles in the coarse mode (Formenti et al., 2018). Briefly, it is based on the  
129 total and polarized radiances measured at 670 and 865 nm. Using a look up table (LUT) built on aerosol  
130 microphysical models (described in Table S1 in the Supplement of Formenti et al., 2018), the algorithm  
131 recalculates for each clear sky pixel the observed polarized radiances at several observational angles. Importantly,  
132 in the aerosol models used for the inversion, aerosols are considered as non-absorbing (the imaginary part of the  
133 refractive index is assumed as zero) and the real part of their refractive index is invariant between 670 and 865  
134 nm. The aerosol number size distribution is lognormal and bimodal with an effective diameter smaller (larger)  
135 than  $1.0 \mu\text{m}$  for the fine (coarse) mode. The coarse mode includes a non-spherical fraction based on the spheroidal  
136 model from Dubovik et al. (2006), whereas a Mie model for homogeneous spherical particles is used to calculate  
137 multi-spectral and multi-angle polarized radiances. As an improvement compared to former versions of the  
138 algorithm, the effective diameter of the spheroidal model is allowed to take two values (namely  $2.96$  and  $4.92 \mu\text{m}$ )  
139 in collection 3 (Table S1 of Formenti et al, 2018). Within the coarse mode, the non-spherical fraction is set to 5  
140 discrete values (0.00, 0.25, 0.50, 0.75, and 1.00, Tanré et al. (2011)). A quality flag index (0 indicating the lowest  
141 and 1 the highest quality) is attributed to each superpixel depending on the inversion quality. As in Formenti et al.  
142 (2018), only POLDER-3 aerosol products derived from pixels with a quality flag  $\geq 0.5$  have been considered in  
143 our analysis. In the present study, we focus on the western Mediterranean region, west of longitude  $20^\circ\text{E}$ ,  
144 considering the main aerosol parameters derived by POLDER-3 ocean operational algorithm: (i) available for all  
145 clear sky pixels: total, fine, and coarse aerosol optical depth (respectively AOD,  $\text{AOD}_F$ , and  $\text{AOD}_C$ ) at 865 nm,  
146 and Angström Exponent between 670 and 865 nm (AE), (ii) available only when the geometrical conditions are  
147 optimal (scattering angle range of roughly  $90^\circ$ - $160^\circ$ ): spherical and non-spherical fractions of the AOD in the  
148 coarse mode ( $f_{CS}$  and  $f_{CNS}$  respectively), allowing to assess  $\text{AOD}_{CS}$  and  $\text{AOD}_{CNS}$  (spherical and non-spherical  
149 coarse AOD, respectively) at 865 nm. The quality of these POLDER-3 derived aerosol parameters has been  
150 evaluated over the region of interest by Formenti et al. (2018), using co-located in situ airborne measurements  
151 from summer 2012 and 2013 field-experiments and coincident ground-based AERONET data available from 17  
152 insular and coastal sites over the whole POLDER-3 operation period (2005-2013). This first comprehensive  
153 regional evaluation has provided new assessments of uncertainties and highlighted the good quality of collection  
154 3 POLDER-3 aerosol data set over our area of interest (Table 4 of Formenti et al., 2018). In our regional analysis  
155 of spatial distribution and temporal variability of POLDER-3 aerosol retrievals, the AOD,  $\text{AOD}_F$ , and  $\text{AOD}_C$   
156 derived at 865 nm will be complemented, through an extrapolation with the Angström Exponent, by those at 550  
157 nm, which is the standard wavelength of many aerosol satellite retrievals and model simulations (Nabat et al.,  
158 2013).

## 159 **3 Results**

### 160 **3.1 Mean regional and seasonal picture (2005-2013)**

163 The climatological (March 2005 – October 2013) seasonal maps of POLDER-3 derived AOD, AE,  $\text{AOD}_F$ ,  $\text{AOD}_C$ ,  
164  $\text{AOD}_F/\text{AOD}$  (i.e. Fine Mode Fraction or FMF),  $\text{AOD}_{CNS}$ , and  $\text{AOD}_{CS}$  at 865 nm over marine areas in the region

165 30-50°N, 10°W-20°E, i.e. mainly the western Mediterranean Sea, are shown in Figure 1. The total AOD (left  
166 panels) exhibits a pronounced seasonality with minimum values in winter (defined by the December-January-  
167 February months):  $AOD < 0.10$  over most of the region of study. In spring (March-April-May), AOD shows an  
168 increase, especially intense over the southeastern part of the region between Italy and Africa, whereas the  
169 maximum AOD values ( $\geq 0.20$ ) are reached in summer (June-July-August) over the whole southern part of the  
170 area. In autumn (September-October-November), the AOD over the region are mostly low, comparable to winter  
171 loads, except over the southeastern part of the domain, especially over the Ionian Sea, and off the coast of Tunisia,  
172 Lybia and south of Sicily, where they reach moderate values (range 0.10 – 0.15). This area of enhanced aerosol  
173 transport is geographically similar to that associated to maximum AOD ( $\sim 0.20$ ) in spring. In general, the seasonal  
174 POLDER-3 total AOD maps exhibit a well-established south-to-north gradient, with a decrease of values toward  
175 the northern part, reflecting the high influence of aerosol sources from the North African continent. This aerosol  
176 spatial distribution is consistent with that derived by other satellite sensors over the Mediterranean basin (for  
177 example Moulin et al., 1998, Barnaba and Gobi, 2004; Papadimas et al., 2008). The  $AE_{865-670\text{ nm}}$  seasonal maps  
178 (second column panels) highlight the influence of coarse aerosols (associated with low AE values) in the south  
179 part of the region off the north African coast, and higher contribution of fine particles along the coasts of Europe,  
180 especially over the Adriatic Sea, where AE values are equal or higher than 1, in all seasons.  $AOD_F$ ,  $AOD_C$ , and  
181  $AOD_F/AOD$  (FMF) seasonal maps, shown in the three central column panels, confirm this pattern of spatial  
182 variability, typical of coarse and fine aerosol repartition in the Mediterranean basin. The seasonal and spatial  
183 variability of  $AOD_{CNS}$  is close to that observed for  $AOD_C$ , whereas POLDER-3 retrievals of  $AOD_{CS}$  suggest a  
184 relatively homogeneous repartition of coarse spherical particles, with low values ( $AOD_{CS} < 0.05$ ), and no  
185 substantial spatial and seasonal variations (right panels of Figure 1). Figure S1 of the supplementary material  
186 complements these POLDER-3 seasonal maps at 865 nm, with AOD,  $AOD_F$ ,  $AOD_C$ , and  $AOD_F/AOD$  (i.e. FMF)  
187 extrapolated at 550 nm. At this wavelength, AOD reach higher values ( $\geq 0.30$  during summer maximum), in  
188 agreement with  $AOD_{550\text{ nm}}$  range of retrievals from reference satellite sensors like MODIS and MISR over the  
189 region (Nabat et al., 2013). As expected, POLDER-3  $AOD_F$  are strongly enhanced (values up to 0.16-0.20)  
190 compared to 865 nm ( $< 0.08$ ), whereas  $AOD_C$  values are only slightly modified. These ranges of values are  
191 consistent with the stronger wavelength dependence of AOD of small particles, characterized by high AE values,  
192 inducing pronounced increase of  $AOD_F$  values toward shorter wavelengths. Thus, the spatial distribution of  
193 POLDER-3  $AOD_F$  at 550 nm is characterized by maximum values ( $> 0.10$ ) over the eastern part of the region of  
194 study, and seasonal peaks in spring and summer. North of the Adriatic Sea, POLDER-3 highlights an area  
195 characterized by all-year persistent high values of  $AOD_F$  ( $> 0.12$  at 550 nm), most probably reflecting  
196 accumulation of pollution particles due to influence of regional anthropogenic sources (as for example from  
197 Northern Italy in the Po Valley). Such a spatial pattern is fully consistent with the recent analysis of Hansson et  
198 al. (2021) highlighting that polluted air masses coming from the north along the Adriatic Sea are affecting air  
199 quality in a large part of the Mediterranean.

### 200 201 3.2 Sub-regional features

202 In order to examine more deeply the seasonal variations of POLDER-3 aerosol retrievals accounting for the south-  
203 to-north gradient observed in Figure 1, the area of study has been divided into three main latitudinal sub-regions.  
204 These regions are illustrated in Figure 2. They correspond respectively to the northern part (north of latitude 42°N:

205 zone 1 called NW MED), the central part (latitude band 38 – 42 °N, zone 2 called CW MED), and the southern  
206 part (south of latitude 38°N: zone 3 called SW MED) of the western Mediterranean Sea (6°W- 20°E).  
207 Figure S2 of the supplementary material reports the statistics of the POLDER-3 retrievals over the March 2005-  
208 October 2013 time period in each-sub-region, with mean and standard deviations, maximum and minimum values  
209 of number of available clear-sky superpixels (left column) and number of available days of observations for each  
210 month and year (right column). As expected, more POLDER-3 retrievals are available in summer than in winter  
211 months, due to the higher influence of cloudiness during the cold season. The number of days with aerosol  
212 retrievals by month and year for each sub-region (right column) highlights that more than 50% of daily POLDER-  
213 3 retrievals are available for most of the months of the whole time period. A few exceptions occur for some specific  
214 months, as July 2007 and July 2010, common at the three sub-regions due to missing data during these periods  
215 related to instrumental problems with the solar sensor (only 28% and 14% of data available, respectively). These  
216 statistics suggests that the cloudiness significantly reduces the number of POLDER-3 pixels available over each  
217 sub-region from October to March (Figure S2a,c,e), with more limited impact on number of available days of  
218 POLDER-3 observations (Figure S2b,d,f).

219 Figure 3 illustrates the 8- or 9-year climatological mean over March 2005 – October 2013 of monthly POLDER-  
220 3 derived aerosol parameters at 865 nm over the three sub-regions defined in Figure 2. The averaged seasonal  
221 cycle of AOD is relatively similar over the north and central parts of the basin, whereas the southern part shows  
222 generally higher total aerosol loads, and a more pronounced seasonal variability, with two maxima in April-May  
223 and July (mean  $AOD_{865\text{ nm}} > 0.15$ ). This evolution is consistent with a dominant influence of African dust transport,  
224 which is known to begin over the eastern basin in spring and spread over the western basin in summer (Moulin et  
225 al., 1998; Floutsi et al., 2016). The mean monthly variations of the POLDER-3  $AOD_F$  integrated over the three  
226 sub-regions are remarkably similar, in agreement with previous analysis based on ground-based AERONET  
227 observations suggesting that the aerosol fine mode is, to some extent, relatively homogeneously distributed over  
228 the western Mediterranean region (Lyamani et al., 2015; Sicard et al., 2016). Conversely, the north-south gradient  
229 clearly appears for  $AOD_C$  (right column middle panel of Figure 3), especially for the SW MED area, consistently  
230 with what is observed for total AOD. The seasonal variations of the monthly-averaged AE (left column middle  
231 panel) reflect the north–south gradient of aerosol sizes, with an increased influence of smaller particles toward the  
232 north, a pattern confirmed by the monthly evolution of FMF (left column, bottom panel). The monthly-averaged  
233  $AOD_{CS}$  (right column, bottom panel) shows very low seasonal and spatial variability, as previously observed in  
234 Figure 1, whereas the POLDER-3 mean  $AOD_{CNS}$  seasonal cycle illustrates much more pronounced monthly and  
235 north-south evolution, in coherence with those of  $AOD_C$  and total AOD. Figure S3 in the supplementary material  
236 illustrates the climatological mean of monthly POLDER-3 AOD,  $AOD_F$ ,  $AOD_C$ , and FMF extrapolated at 550 nm,  
237 confirming the patterns displayed Figure 1, especially the marked increase of  $AOD_F$  values, and FMF at this  
238 wavelength. Thus, POLDER-3 FMF (550 nm) are consistent with previous averaged estimates from MODIS over  
239 Western Mediterranean, ranging from 55 to nearly 70% (Floutsi et al., 2016).

240 The POLDER-3 mean seasonal aerosol retrievals displayed in Figure 1 and 3 at 865 nm are summarized in Table  
241 1a, those extrapolated at 550 nm (Figures S1 and S3) in Table 1b. The multi-annual averages of AOD,  $AOD_C$  and  
242  $AOD_{CNS}$  at 865 nm in Table 1a confirm the north-south gradient with minimum values in the north part (0.090,  
243 0.055, and 0.043 respectively for AOD,  $AOD_C$ , and  $AOD_{CNS}$ ) compared to the south part of the western  
244 Mediterranean basin (0.124, 0.091, 0.073 respectively). POLDER-3 AE and FMF mean multi-annual values

245 consistently highlight an increase in the coarse component of AOD toward the south. In terms of multi-annual  
246 averages, the AOD<sub>F</sub> remains relatively uniform, with some minor variations indicating minimum fine mode  
247 aerosol loads in the central area (0.032 in CW MED), maximum in the north (0.035 in NW MED) and intermediate  
248 values in the south part (0.033 in SW MED), these variations being more pronounced at 550 nm (Table 1b).  
249 Seasonal multi-annual averages of AOD<sub>F</sub> highlight differences in the order of a factor 2 between minimum values  
250 in the south in winter (around 0.02 at 865 nm, 0.06 at 550 nm) and maxima in spring (around 0.04 at 865 nm, and  
251 0.12 at 550 nm), especially in the northern part of the region. The POLDER-3 derived mean multi-annual AOD<sub>CS</sub>  
252 at 865 nm (Table 1a) reveal some seasonal variability, with maximum values in summer in the south part (0.031)  
253 and minimum in winter in the northern part (0.013). Although reasons for such an evolution are not fully  
254 understood, considering the similarity with that of AOD<sub>CNS</sub>, this variability could be partly related to the influence  
255 of North African dust transport rather than fully representative of a background coarse sea-salt fraction (Claeys et  
256 al., 2017). Indeed, Saharan dust might include a spherical coarse aerosol fraction following mixing with soluble  
257 secondary components such as sulfate and nitrate (Drugé et al., 2019).

### 258 259 **3.3 Temporal evolution at selected sites**

260  
261 The previous regional analysis is complemented by the investigation of the POLDER-3 aerosol properties around  
262 three contrasted AERONET sites of the western basin: Ersa (43.00367°N, 9.35929°E, altitude 80 m), the  
263 northernmost site located on northern coast of Corsica Island, France; Lampedusa (35.51667°N, 12.63167°E, alt.  
264 45 m) the southernmost site located on the northwestern coast of Lampedusa Island, Italy; Barcelona (41.38925°N,  
265 2.11206°E, alt. 125 m) the westernmost site located in a urban/coastal environment on the shore of northeastern  
266 Spain (Figure 2). Ersa and Barcelona are sites under the influence of long-range Saharan dust transport, whereas  
267 Lampedusa is subject to short to medium-range dust transport. Ersa and Lampedusa are marine background sites  
268 with some anthropogenic influence, Barcelona is located in a heavily polluted environment. Ersa and Lampedusa  
269 were the two super-sites of the ChArMEx (The Chemistry-Aerosol Mediterranean Experiment) collaborative  
270 research program, and Barcelona, which is also part of EARLINET/ACTRIS network, one of the secondary sites  
271 of this program (Mallet et al., 2016). In this context, the long-term AERONET routine aerosol measurements at  
272 these sites have been used for the comprehensive regional validation of POLDER-3 retrievals presented in  
273 Formenti et al. (2018). Here we considered the same POLDER-3 dataset, by selecting superpixels within  $\pm 0.5^\circ$   
274 around the AERONET sites, corresponding to a maximum number of 17 at Ersa, 28 at Lampedusa, and 13 at  
275 Barcelona.

#### 276 277 **3.3.1 Monthly time series**

278 Figure 4, 5 and 6 illustrate the month-to-month evolution from March 2005 to October 2013 of POLDER-3  
279 retrievals at 865 nm, extracted at Ersa, Barcelona and Lampedusa respectively, including (a) AOD, (b) AOD<sub>F</sub> and  
280 AOD<sub>C</sub>, (c) AOD<sub>CNS</sub> and AOD<sub>CS</sub>, (d) AE<sub>865-670</sub> and FMF. At these three sites, AE and FMF (Figure 4d, 5d, 6d) show  
281 remarkably similar variability (correlation coefficients  $r > 0.9$ ), indicating that the AE is a good proxy of the  
282 proportion of fine particles component relative to total AOD.

283 The average monthly FMF of the AOD at 865 nm at Ersa is estimated at 37% by POLDER-3 in all clear-sky  
284 conditions, with a range of monthly mean values between 18% and 65%. Consistently, considering only the  
285 POLDER-3 retrievals available in Best Viewing Conditions, the averaged repartition in terms of aerosol size mode

286 and shape contributions to the total AOD at 865 nm at Ersa are 36% for the fine AOD, 44% for the non-spherical  
287 coarse mode and 20% for the spherical coarse mode.

288 As a consequence of the influence of short to medium range Saharan dust transport in Lampedusa, POLDER-3  
289 AOD show their highest monthly mean values at this site (up to 0.44 in May 2011, Figure 6a), compared to both  
290 Ersa (max of 0.21 in June 2007, Figure 4a) and Barcelona (max of 0.24 in June 2006, Figure 5a). These maximum  
291 AOD values are associated to coincident maximum values of monthly mean AOD<sub>C</sub>, with 0.39 in May 2011 in  
292 Lampedusa (Figure 6b), 0.18 in June 2006 in Barcelona (Figure 5b), and 0.16 in June 2007 in Ersa (Figure 4b).  
293 Figures 4-6 highlight that POLDER-3 monthly mean AOD values above 0.10 are much more frequent in  
294 Lampedusa (66% of frequency over the 104 months of POLDER-3 observations) than in Barcelona (43% of  
295 frequency) and Ersa (30%). The contrast between the three sites is even more pronounced considering the AOD<sub>C</sub>  
296 retrievals, with frequencies of monthly values above 0.10 reaching 44%, 22%, and 5% for Lampedusa, Barcelona,  
297 and Ersa, respectively. Conversely, the monthly evolution of AOD<sub>F</sub> reported in Figure 4b, 5b, and 6b does not  
298 show such a marked contrast, nor with respect to the maximum values (0.072, 0.074, and 0.076 in Ersa, Barcelona,  
299 and Lampedusa, respectively), or the frequency of monthly mean values above 0.04 (27%, 31% and 34%  
300 respectively).

301 The months with POLDER-3 mean derived FMF greater than 50% represent a frequency of 10% over the whole  
302 monthly data set in Barcelona (Figure 5d), and 0% in Lampedusa (Figure 6d). Compared to their frequency in Ersa  
303 (17%, Figure 4d), POLDER-3 retrievals suggest that the influence of fine particles is more frequent in Ersa,  
304 possibly due to the transport of polluted air masses from highly industrialized regions (Po Valley, Marseille-Fos-  
305 Berre for example) in the north part of the basin (Mallet et al., 2016). These features could also reflect the high  
306 influence of desert dust at Lampedusa and in a less extent at Barcelona, which may partly hide the possible  
307 influence of fine aerosols of anthropogenic origin at these two sites.

308 Over the whole POLDER-3 observing period, maximum monthly mean values of AOD<sub>CS</sub> range from 0.058 in Ersa  
309 (March 2008, Figure 4c) to 0.075 in Lampedusa (April 2008, Figure 6c) and 0.090 in Barcelona (November 2009,  
310 Figure 5c). Frequencies of monthly mean POLDER-3 AOD<sub>CS</sub> values above 0.03 are 13%, 31%, and 38% at Ersa,  
311 Barcelona, and Lampedusa respectively. Such a variability suggests some impact of desert dust on AOD<sub>CS</sub>,  
312 although the contribution of sea-salt particles or a combination of both aerosol types cannot be excluded.  
313 Maximum monthly AOD<sub>CNS</sub> values range from 0.109 at Ersa (Sept. 2008 and May 2009, Figure 4c) to 0.210 at  
314 Barcelona (Nov. 2009, Figure 5c) and 0.220 at Lampedusa (March 2005, Figure 6c). Frequencies of monthly mean  
315 POLDER-3 AOD<sub>CNS</sub> values above 0.03 reach 91% in Lampedusa, 70% in Barcelona, and 67% in Ersa.  
316 Considering only the POLDER-3 retrievals available in Best Viewing Conditions, the averaged contributions in  
317 terms of aerosol size and shapes at Barcelona are quite similar to those estimated at Ersa, with 34% of fine AOD,  
318 46% of coarse non-spherical AOD and 20% of coarse spherical AOD at 865 nm. At Lampedusa, the averaged  
319 contribution of fine AOD is reduced to 26%, with a higher contribution of coarse non-spherical AOD (55%), and  
320 a rather constant relative contribution of coarse spherical AOD (19%).

### 321 322 **3.3.2 Daily time series** 323

324 Figure 7 shows the frequency distributions for daily POLDER-3 AOD (a), AOD<sub>F</sub>(b), AOD<sub>C</sub>(c), AOD<sub>CNS</sub> (d), and  
325 AOD<sub>CS</sub> (e) at 865 nm at Ersa, Barcelona, and Lampedusa, their daily evolutions from March 4, 2005 to October  
326 10, 2013 being reported in Figure S4 of the supplementary material. Table 2 presents a statistical summary of the  
327 daily POLDER-3 aerosol retrievals for these three sites.



328 The range of AOD values varies from 0.01 to 0.68 at Ersa, 0.01 to 1.05 at Barcelona, and 0.02 to 4.72 at  
329 Lampedusa, indicating the occurrence of extreme AOD events at the southernmost site of Lampedusa. Daily AOD  
330  $> 0.3$  occur 9% of the time in Lampedusa, less than 3% of the time in Barcelona and are rare in Ersa (1.5 % of  
331 frequency). At the three sites, they are characterized by comparable size/shape properties typical of desert dust  
332 influence (low AE and FMF, dominant non-spherical aerosol fraction in the coarse mode). These POLDER-3  
333 retrievals are consistent with the Gkikas et al. (2013) climatology of intense desert dust events in the  
334 Mediterranean, which recorded extreme dust episodes mostly in the southern part of central Mediterranean, where  
335 Lampedusa is located, with  $AOD_{550nm}$  values  $> 2.5$  and up to 4.

336 The background aerosol conditions, corresponding to low POLDER-3  $AOD_{865 nm}$  ( $< 0.05$ ) show an average  
337 occurrence of 22% of the time in Ersa, 20% in Barcelona and only 9.5% in Lampedusa. These features show that,  
338 over the March 2005 – October 2013, POLDER-3 has recorded very low occurrence of pristine days, i.e., clean  
339 conditions associated to low aerosol loads, especially at Lampedusa.

340 As reported in Table 2, the average daily AOD (865 nm) is 0.09 (standard deviation 0.07) in Ersa, 0.10 (standard  
341 deviation 0.04) in Barcelona, and 0.15 (standard deviation 0.18) in Lampedusa, reflecting both higher frequency  
342 and intensity of aerosol episodes in Lampedusa, as illustrated in Figure S4a. This is also verified for POLDER-3  
343 retrievals of  $AOD_c$  and to a certain extent  $AOD_F$ , which reach their maximum values in Lampedusa (4.4 and 0.35,  
344 respectively). However, POLDER-3 shows that at 865 nm, the  $AOD_F$  is always lower than 0.2 (Figure S4b), except  
345 at Lampedusa for a reduced number of days (4). At this site, peaks of  $AOD_F$  seem to be associated to peaks of  
346  $AOD_c$ , suggesting the influence of desert dust on both aerosol size components, and/or the double influence of  
347 two different aerosol types (i.e., possibly both dust and anthropogenic). POLDER-3  $AOD_{CS}$  and  $AOD_{CNS}$  time  
348 series, shown Figure S4d, are more difficult to interpret, because of sampling reduction by more than 50%  
349 compared to POLDER-3 retrievals associated to all clear sky pixels (ACSP, i.e., AOD,  $AOD_F$ ,  $AOD_c$ , AE), due  
350 to the necessity of best viewing conditions (BVC) for their retrieval, as reported in Table 2. Despite this limitation,  
351 Figure S4d and Table 2 show high variability of both spherical and non-spherical aerosols in the coarse mode,  
352 with a larger range of daily values for  $AOD_{CNS}$  (up to 1.00 in Lampedusa) than for  $AOD_{CS}$  (maximum 0.34 in  
353 Barcelona). Considering the three sites, POLDER-3 mean retrievals of daily  $AOD_{CNS}$  (0.04 – 0.08) are on average  
354 more than two times larger than those of  $AOD_{CS}$  (0.02 – 0.03).

### 355 356 **3.4 Inter-annual evolution** 357

358 Annual maps of POLDER-3 AOD,  $AOD_c$ , and  $AOD_F$  at 865 nm are displayed for each of the 9 available  
359 observations years (2005 to 2013) in Figure 8. The annual averages are computed over the period March-October  
360 only in order to consistently consider the 9 years in the whole available period. The left period November-February  
361 is hopefully the period where AOD is the lowest in the region (Figure 3). Figure 8 highlights a significant  
362 interannual variation in AOD (left column), characterized by elevated aerosol loads for specific years, as 2007 and  
363 2008, and lower AOD ranges in 2009 and 2013. The interannual variations of POLDER-3  $AOD_c$  (middle column)  
364 tend to be relatively similar to those of AOD, especially over the south part of the basin. Figure 8 also suggests  
365 that the maximum values of  $AOD_F$  (right column) were observed in the first half of the period of study, with an  
366 evolution toward more moderate to low loads in fine particles apparent from 2010. Figure S5 of the supplementary  
367 material confirms such an evolution with annual maps of POLDER-3  $AOD_F$  extrapolated at 550 nm for each of  
368 the 9 observation years. The year 2007 appears highly polluted in fine particles over the whole basin. Over the

369 most eastern part of the region, the intense plume observed by POLDER-3 can be related to the occurrence of  
370 devastating fires in Greece in the summer of 2007, producing large amounts of biomass burning aerosols  
371 transported downwind over the central Mediterranean (Kaskaoutis et al., 2011).

372 In order to analyze further these interannual evolutions, Figure 9 presents the time series of annual averages of  
373 POLDER-3 AOD, AOD<sub>F</sub>, and AOD<sub>C</sub> at 865 nm spatially averaged over the north, central, and south parts of the  
374 western Mediterranean basins (left column, defined in Figure 2) and extracted at Ersa, Barcelona, and Lampedusa  
375 (right column) for the period March 2005 – October 2013. The associated monthly anomalies, computed by  
376 subtracting to each monthly averaged value of a specific year its corresponding long-term monthly average (2005-  
377 2013) are shown in Figure S6 of the supplementary material. Linear regressions are applied to both March-October  
378 annual averages and monthly anomalies of POLDER-3 AOD, AOD<sub>F</sub>, and AOD<sub>C</sub> evolution as a function of time.  
379 The values of the slopes, reported in Table 3 and Table 4 provide the sign and magnitude of the trends at 865 nm.  
380 Slopes derived from the same analysis of POLDER-3 AOD, AOD<sub>F</sub>, and AOD<sub>C</sub> extrapolated at 550 nm are reported  
381 in Table S1 and Table S2 of supplementary material.

382 Overall, this analysis reveals negative values of the trends for all the sub-regions and sites considered over our  
383 study region, highlighting that POLDER-3 has recorded a general decrease of aerosol loads over western  
384 Mediterranean Sea over the period 2005-2013. The decreasing trends recorded for AOD interannual evolution are  
385 found to be statistically significant, at least at the 95% confidence level, over the northern and central part of the  
386 study region and, consistently, at Ersa and Barcelona (top panels of Figure 9). AOD<sub>C</sub> interannual evolutions  
387 recorded by POLDER-3 suggest decreasing trends, although the confidence level of 95% is only reached when  
388 considering monthly anomalies at Barcelona and for the three sub-regions (Table 3). The absolute values of the  
389 POLDER-3 AOD<sub>C</sub> decreasing trends, especially in the northern part of the basin (NW MED, trend - 0.0012 yr<sup>-1</sup>)  
390 suggest a moderate-to-low decreasing tendency, around -0.01 per decade. Interestingly, POLDER-3 AOD<sub>F</sub>  
391 interannual evolutions for the three sub-regions (bottom panels of Figure 9 and S6) clearly reveal robust decreasing  
392 trends, all statistically significant at 99% level (Student's test). As reported in Table 3, considering the northern  
393 and central parts of the study region, AOD<sub>F</sub> decreased by - 0.0020 yr<sup>-1</sup> at 865 nm (- 0.005 yr<sup>-1</sup> at 550 nm, Table  
394 S1) whereas the decrease found in the southern part is slightly lower, - 0.0016 yr<sup>-1</sup> at 865 nm ( $\leq$  - 0.004 yr<sup>-1</sup> at 550  
395 nm, Table S1). POLDER-3 AOD<sub>F</sub> interannual variability at Ersa, Barcelona, and Lampedusa confirm these  
396 downward evolutions, with decreasing trends statistically significant at the 99% confidence level (Table 4). The  
397 decrease trends seem to be more pronounced in Barcelona ( $\geq$  - 0.0026 yr<sup>-1</sup>) than in Lampedusa ( $\geq$  - 0.0015 yr<sup>-1</sup>),  
398 with intermediate magnitudes at Ersa ( $\geq$  - 0.0019 yr<sup>-1</sup>). Consistently, the decreasing trends derived from POLDER-  
399 3 AOD<sub>F</sub> extrapolated at 550 nm vary between values around - 0.007 yr<sup>-1</sup> at Barcelona, - 0.005/ - 0.006 yr<sup>-1</sup> in Ersa,  
400 and -0.004 yr<sup>-1</sup> in Lampedusa (Table S2). The POLDER-3 AOD<sub>F</sub> marked decreasing in Barcelona is fully  
401 consistent with surface particulate concentrations (PM) downward trend analysis in Spain provided by Querol et  
402 al. (2014) and Pandolfi et al. (2016) over comparable time periods (2001-2012 and 2004-2014 respectively).  
403 Although Querol et al. (2014) discuss effects of meteorological variability and 2008 financial crisis, their main  
404 interpretation is the effect of major policy actions on air quality.

405 The year-to-year variations in the North Atlantic Oscillation (NAO) have been examined in several past studies to  
406 support interpretation of inter-annual changes of north African dust transport either recorded by different satellite  
407 sensors, especially over the Mediterranean in the 1990s and early 2000s decades (Moulin et al., 1997; Antoine et  
408 Nobileau, 2006) or simulated by regional models (Nabat et al, 2020). In the present paper, we investigate the

409 relationship between winter (December through March) NAO index defined by Hurrell (1995) and interannual  
410 variations of POLDER-3 AOD, AOD<sub>F</sub>, and AOD<sub>C</sub> from 2005 to 2013 over the three western Mediterranean sub-  
411 regions and sites considered in this work. The winter NAO indexes for the 2005–2013 period were obtained from  
412 "The Climate Data Guide: Hurrell North Atlantic Oscillation (NAO) Index (station-based)"  
413 (<https://climatedataguide.ucar.edu/climate-data/hurrell-north-atlantic-oscillation-nao-index-station-based>). The  
414 annual means of POLDER-3 AOD and AOD<sub>F</sub> do not show any statistically significant correlation with the winter  
415 NAO Index, although the correlation coefficients for annual AOD reach 0.51 at Ersa, and 0.66 for CW MED. The  
416 annual averages of AOD<sub>C</sub> confirm a link with the NAO for the CW MED region ( $r=0.70$ , with 95% confidence  
417 level). At Ersa, we obtain  $r=0.54$  which is not significant. These correlation levels, not observed in the southern  
418 areas of our study region (Lampedusa or SW MED), strongly suggest that the NAO exerts a control on north  
419 African dust transport rather than on their emissions over source-regions. In order to go further, we examine the  
420 relative frequency of desert dust episodes ( $f_D$ ) by selecting the days associated with POLDER-3 AOD<sub>C</sub> 865 nm  $\geq$   
421 0.10 for the three-sub regions considered in our study. Figure 10 reports the results for the period 2005–2013  
422 (March–October) along with the time series of the winter NAO Index. A significant correlation is confirmed  
423 between NAO Index and  $f_D$  for the central part of the western Mediterranean region (blue curve,  $R=0.76$ , with  
424 95% confidence level) and to a lesser extent for the northern part of the western Mediterranean region (green  
425 curve,  $R=0.65$ , not significant). For the southern part of the region, the correlation is much lower ( $r=0.43$ ) although  
426 some connection with NAO is apparent at the beginning of the period (2005–2009), the correlation being strongly  
427 degraded by the opposition observed in 2010 between extremely low NAO index (-4.64) and a relatively high  $f_D$   
428 value (36%). It is noticeable that Salvador et al. (2014), in their analysis of interannual variations of African dust  
429 outbreaks for years 2001–2011 over the western Mediterranean basin, excluded the year 2010 from their  
430 correlation plots with NAO indexes considering that it was associated to an atypical low value of the NAO index,  
431 most probably governed by anomalous atmospheric patterns. Interestingly, SW MED is the only of our three  
432 regions where POLDER-3 has recorded a significant decreasing trend in  $f_D$  of -2% ( $\pm 1\%$ ) per year over the period  
433 2005-2013 ( $R=0.68$ , with 95% confident level).

434 Conversely, we also consider the relative frequency of occurrence of clean conditions associated to low aerosol  
435 loads recorded by POLDER-3 at 865 nm for the fine fraction (daily AOD<sub>F</sub> < 0.05), the coarse fraction (daily AOD<sub>C</sub>  
436 < 0.05) and the total aerosol (daily AOD  $\leq 0.10$ ), named  $f_{CF}$  (Clean Fine),  $f_{CC}$  (Clean Coarse), and  $f_{CT}$  (Clean  
437 Total), respectively. Figure 11 reports the year-to-year evolutions of  $f_{CF}$  (top panels),  $f_{CC}$  (middle panels), and  $f_{CT}$   
438 (bottom panels) for the three sub-regions, NW MED, CW MED, SW MED (left column) and Ersa, Barcelona,  
439 Lampedusa (right column). Clearly, POLDER-3 record an increasing trend in the frequency of occurrence of clean  
440 conditions for the fine fraction of AOD, both for the three sub-regions and three sites. The  $f_{CF}$  trends vary between  
441 +2% per year (SW MED and Lampedusa), +3% per year (CW MED, NW MED, Ersa) and +4% per year  
442 (Barcelona), with confidence levels of 99% (except for SW MED where only 95% confidence level is reached).  
443 In Barcelona, the increase is spectacular with clean conditions in fine particles occurring less than 60% of the time  
444 between 2005 and 2007 (minimum in 2007, with 51% of frequency) and reaching values above 75% in the 2011-  
445 2013 years (maximum in 2013, with 85% of frequency). Such an evolution is consistent with decreasing trends in  
446 surface PM<sub>2.5</sub> at background sites in Spain and Europe reported in the literature over 2002–2010 (Cusack et al.,  
447 2012). Pandolfi et al. (2016) further observed decreasing trends between 2004 and 2014 in northeastern Spain,  
448 both at the background site of Barcelona and at the regional background site of Montseny, and mostly related them

449 to decreases in industrial emissions and in secondary sulfate and nitrate fine particle concentrations. Regarding the  
450 coarse fraction of AOD,  $f_{CC}$  records some significant year-to-year variability but no tendency, except for the SW  
451 MED sub-region where a low, slightly positive trend ( $< +1\%$  per year, not significant) is recorded over the period  
452 2005–2013, suggesting a possible slow evolution toward cleaner conditions for the coarse aerosol fraction in the  
453 southern part of the basin. Considering the total aerosol loads (bottom panels of Figure 11),  $f_{CT}$  evolution shows  
454 an increasing trend (between  $+2$  and  $+3\%$  per year with a 95% confidence level) for the three sub-regions and  
455 three sites considered.

456 Figure 12 and Figure 13 compare the 2005-2013 (March - October) mean values of  $AOD_F$  and  $AOD_C$  respectively  
457 with their anomalies for each year of the period. The year-to-year evolution of  $AOD_F$  is clearly characterized by  
458 positive anomalies in the first years of the period of study (especially, 2005-2007), and negative anomalies for the  
459 most recent years. The spatial distributions of these anomalies indicate lower than long term means  $AOD_F$  over  
460 the eastern part of the region in 2012, and mostly over the northern and western part of the region in 2013. Annual  
461 anomalies of  $AOD_C$  illustrated in Figure 13 highlight elevated loads of coarse aerosols for specific years and areas  
462 of the region, as in 2008 in the southeastern part or in 2012 in the western part of the basin. In contrast, 2009  
463 (southeastern part), 2010 (western part), and 2013 (most of the basin) appear to be associated with lower than  
464 long-term means values of  $AOD_C$ . These POLDER-3 interannual evolutions tend to confirm the association  
465 between increased dust transport during positive NAO phases ( $+2.1$  in 2008,  $+3.17$  in 2012) and reduced dust  
466 export in negative NAO phases ( $-4.64$  in 2010,  $-1.97$  in 2013), in agreement with former studies over the region  
467 (Moulin et al., 1997; Antoine and Nabileau, 2006; Papadimas et al., 2008).

468

#### 469 **4 Conclusion**

470

471 On the basis of the quality and robustness of the POLDER-3 clear-sky ocean operational aerosol retrievals over  
472 the western Mediterranean (Formenti et al., 2018), in this paper we investigated the spatial patterns and temporal  
473 variability of the POLDER-3 AOD in different particle size classes (total, fine and coarse components) and shapes  
474 (coarse spherical and non-spherical contributions) over its whole observing period 2005-2013.

475 The POLDER-3 aerosol record confirms the high influence of north African desert dust over the region, with a  
476 marked maximum in AOD, along with its coarse and coarse non-spherical component in the southernmost part,  
477 associated with a decrease in AE and fine mode fraction (FMF), and a seasonal maximum occurring in Spring and  
478 Summer. In contrast, the coarse spherical component of AOD remains relatively homogeneously low all year long  
479 over the region ( $AOD_{CS} < 0.05$ ). The POLDER-3 retrievals of the fine component of AOD show moderate spatial  
480 variability, with larger  $AOD_F$  in the eastern part of our region of study, especially north of the Adriatic Sea. At  
481 three sites representative of different typical aerosol conditions over the western Mediterranean Sea (namely Ersa,  
482 Barcelona, and Lampedusa), POLDER-3 retrievals indicate averages contributions to total AOD at 865 nm ranging  
483 between 19 and 20% for coarse spherical particles, 26 and 36% for fine particles (maximum at Ersa), and 44 and  
484 55% for coarse non-spherical particles (maximum at Lampedusa). At Lampedusa, POLDER-3 daily observations  
485 record the occurrence of intense or extreme aerosol events ( $AOD > 1$  up to 4.7) consistently with the higher and  
486 more direct influence of severe desert dust episodes at this southernmost site. At these three sites, daily POLDER-  
487 3  $AOD_{865\text{ nm}}$  values above 0.3 are associated with low AE and FMF (mean values below 0.5 and 21%, respectively),  
488 as well as a dominance of the non-spherical particle fraction in the coarse mode (mean values above 71%), typical

489 of the desert dust influence. The background “clean” conditions associated to very low aerosol loads (POLDER-3  
490 daily AOD<sub>865 nm</sub> values below 0.05) occur 22% of the time around Ersa, 20% around Barcelona and 9.5% around  
491 Lampedusa over the POLDER-3 period (2005-2013), highlighting the scarcity of pristine days in this region,  
492 especially in its southern part.

493 Our analysis shows that the interannual evolutions of AOD, AOD<sub>F</sub> and AOD<sub>C</sub> have negative trends over the period  
494 2005-2013, more pronounced in time and space for AOD<sub>F</sub> than for the AOD<sub>C</sub>/AOD components. On average the  
495 POLDER-3 AOD decreased by 0.0030 per year at 865 nm (0.0060 per year at 550 nm) over most of the region,  
496 with high contributions of decreasing fine mode AOD (-0.0020 per year at 865 nm, -0.0050 per year at 550 nm).  
497 These decreasing tendencies are consistent with those reported in previous studies based on MODIS AOD at 550  
498 nm, ranging from -0.0030 per year (over 2002-2014, Floutsi et al., 2016) and -0.0067 per year (over 2000-2006,  
499 Papadimas et al., 2008). We suggest a link between inter-annual evolution of winter NAO Index and frequency of  
500 desert dust episodes (POLDER-3 AOD<sub>C</sub> at 865 nm greater than 0.10, f<sub>D</sub>), especially over the central part of the  
501 western Mediterranean Sea, along with a possible moderate diminution of frequency of dust spatially limited to  
502 the south basin, as also indicated by Floutsi et al. (2016).

503 Our results strongly support the significant improvement in air quality for the fine mode aerosol component over  
504 the western Mediterranean region, with much less evidence of such a large-scale evolution for the coarse fraction.  
505 POLDER-3 analysis shows that aerosol year-to-year evolution over the period 2005-2013 is marked by significant  
506 positive trends of occurrences of clean conditions in terms of fine particles (classified as AOD<sub>F</sub> 865 nm below  
507 0.05), between +2 and +4% per year over the whole region. In Barcelona, for instance, clean conditions recorded  
508 by POLDER-3 AOD<sub>F</sub> were as frequent as 75% in the period 2010-2013.

509 Overall, our analysis contributes to emphasize the capacity of evolved aerosol dedicated satellite dataset in  
510 distinguishing multi-influenced pluri-annual evolutions in regions undergoing complex aerosol contributions, as  
511 in the Mediterranean basin. Such an approach may be investigated in other climate-sensitive regions of the world,  
512 subjected to specific anthropogenic pressures and meteorological patterns. In the Mediterranean, this POLDER-3  
513 data set will be part of the validation exercise of regional climate model analysis in the framework of the Flagship  
514 Pilot Studies of aerosols within CORDEX (Nabat et al., 2013; 2020).

515

#### 516 **Data availability**

517 POLDER-3 data extraction was performed with the program PARASOLASCII ([http://www-loa.univ-](http://www-loa.univ-lille1.fr/~ducos/public/parasolascii/)  
518 [lille1.fr/~ducos/public/parasolascii/](http://www-loa.univ-lille1.fr/~ducos/public/parasolascii/)). This version is made available from the AERIS Data and Service Center  
519 (<http://www.icare.univ-lille1.fr/parasol>). Technical details are described at [http://www.icare.univ-](http://www.icare.univ-lille1.fr/projects_data/parasol/docs/Parasol_Level-2_format_latest.pdf)  
520 [lille1.fr/projects\\_data/parasol/docs/Parasol\\_Level-2\\_format\\_latest.pdf](http://www.icare.univ-lille1.fr/projects_data/parasol/docs/Parasol_Level-2_format_latest.pdf). The definition of the flag index is detailed  
521 at page 18 (parameter: quality of the fit).

#### 522 **Competing interests**

523 FD is guest editor for the ACP Special Issue of the Chemistry and Aerosols Mediterranean Experiment (ChArMEX)  
524 (ACP/AMT inter-journal SI)”. The remaining authors declare that they have no conflict of interest.

#### 525 **Special issue statement**

526 This article is part of the special issue of the Chemistry and Aerosols Mediterranean Experiment (ChArMEX)  
527 (ACP/AMT inter-journal SI)”. It is not associated with a conference.

528

529 **Acknowledgements**

530 This work is part of the ChArMEx project supported by CNRS-INSU, ADEME, Météo-France and CEA in the  
531 framework of the multidisciplinary program MISTRALS (Mediterranean Integrated Studies aT Regional And  
532 Local Scales; <http://mistrals-home.org/>). It has also been supported by the French National Research Agency  
533 (ANR) through the ADRIMED project (contract ANR-11-BS56-0006) and by the French National Program of  
534 Spatial Teledetection (PNTS, <http://www.insu.cnrs.fr/pnts>, project n°PNTS-2015-03). L. Mbemba Kabuiku was  
535 granted by the French Environment and Energy Management Agency (ADEME) and National Center of Space  
536 Studies (CNES). The French national center for Atmospheric data and services AERIS provided access to the  
537 POLDER-3 data used.

538 LOA participates in the CaPPA (Chemical and Physical Properties of the Atmosphere) project funded by the  
539 French National Research Agency (ANR) through the PIA (Programme d'Investissement d'Avenir) under contract  
540 ANR-11-LABX-0005-01, the Regional Council “Hauts-de-France” and the European Regional Development  
541 Fund (ERDF). We would like to thank Marc Mallet and Pierre Nabat (CNRM-Toulouse, France) for fruitful  
542 discussions about the results of this paper.

543

544 **References**

545 Ancellet, G., Pelon, J., Totems, J., Chazette, P., Bazureau, A., Sicard, M., Di Iorio, T., Dulac, F., and Mallet, M.:  
546 Long-range transport and mixing of aerosol sources during the 2013 North American biomass burning episode:  
547 analysis of multiple lidar observations in the western Mediterranean basin, *Atmos. Chem. Phys.*, 16, 4725-4742,  
548 <https://doi.org/10.5194/acp-16-4725-2016>, 2016.

549 Antoine, D., and Nobileau, D.: Recent increase of Saharan dust transport over the Mediterranean Sea, as revealed  
550 from ocean color satellite (SeaWiFS) observations, *J. Geophys. Res. Atmos.*, 111, 1–19,  
551 <https://doi.org/10.1029/2005JD006795>, 2006.

552 Barnaba, F., and Gobbi, G. P.: Aerosol seasonal variability over the Mediterranean region and relative impact of  
553 maritime, continental and Saharan dust particles over the basin from MODIS data in the year 2001, *Atmos. Chem.*  
554 *Phys.*, 4, 2367–2391, <https://doi.org/10.5194/acp-4-2367-2004>, 2004.

555 Boucher, O.: *Atmospheric Aerosols - Properties and Climate Impacts*, 311 pp., Springer,  
556 <https://doi.org/10.1007/978-94-017-9649-1>, 2015.

557 Bréon, F. M., Vermeulen, A., and Descloitres, J.: An evaluation of satellite aerosol products against sunphotometer  
558 measurements, *Remote Sens. Environ.*, 115, 3102–3111, <https://doi.org/10.1016/j.rse.2011.06.017>, 2011.

559 Chazette, P., Totems, J., Ancellet, G., Pelon, J., and Sicard, M.: Temporal consistency of lidar observables during  
560 aerosol transport events in the framework of the ChArMEx/ADRIMED campaign at Menorca Island in June 2013,  
561 *Atmos. Chem. Phys.*, 16, 2863–2875, <https://doi.org/10.5194/acp-16-2863-2016>, 2016.

562 Chazette, P., Totems, J., and Shang, X.: Transport of aerosols over the French Riviera - link between ground-based  
563 lidar and spaceborne observations, *Atmos. Chem. Phys.*, 19, 3885-3904, [https://doi.org/10.5194/acp-19-3885-](https://doi.org/10.5194/acp-19-3885-2019)  
564 [2019](https://doi.org/10.5194/acp-19-3885-2019), 2019.

565 Chrit, M., Sartelet, K., Sciare, J., Pey, J., Nicolas, J. B., Marchand, N., Freney, E., Sellegri, K., Beekmann, M.,  
566 and Dulac, F.: Aerosol sources in the western Mediterranean during summertime: A model-based approach, *Atmos.*  
567 *Chem. Phys.*, 18, 9631-9659, <https://doi.org/10.5194/acp-18-9631-2018>, 2018.

568 Claeys, M., Roberts, G., Mallet, M., Arndt, J., Sellegri, K., Sciare, J., Wenger, J., and Sauvage, B.: Optical,  
569 physical and chemical properties of aerosols transported to a coastal site in the western Mediterranean: a focus on  
570 primary marine aerosols, *Atmos. Chem. Phys.*, 17, 7891–7915, <https://doi.org/10.5194/acp-17-7891-2017>, 2017.

571 Cusack, M., Alastuey, A., Pérez, N., Pey, J., and Querol, X.: Trends of particulate matter (PM<sub>2.5</sub>) and chemical  
572 composition at a regional background site in the Western Mediterranean over the last nine years (2002–2010),  
573 *Atmos. Chem. Phys.*, 12, 8341–8357, <https://doi.org/10.5194/acp-12-8341-2012>, 2012.

574 Denjean, C., Cassola, F., Mazzino, A., Triquet, S., Chevallier, S., Grand, N., Bourriane, T., Momboisse, G.,  
575 Sellegri, K., Schwarzenbock, A., Freney, E., Mallet, M., and Formenti, P.: Size distribution and optical properties  
576 of mineral dust aerosols transported in the western Mediterranean. *Atmos. Chem. Phys.*, 16, 1081–1104,  
577 <https://doi.org/10.5194/acp-16-1081-2016>, 2016.

578 Di Biagio, C., Doppler, L., Gaimoz, C., Grand, N., Ancellet, G., Raut, J.-C., Beekmann, M., Borbon, A., Sartelet,  
579 K., Attié, J.-L., Ravetta, F., and Formenti, P.: Continental pollution in the western Mediterranean basin: vertical  
580 profiles of aerosol and trace gases measured over the sea during TRAQA 2012 and SAFMED 2013, *Atmos. Chem.*  
581 *Phys.*, 15, 9611–9630, <https://doi.org/10.5194/acp-15-9611-2015>, 2015.

582 Di Biagio, C., Formenti, P., Doppler, L., Gaimoz, C., Grand, N., Ancellet, G., Attié, J.-L., Bucci, S., Dubuisson,  
583 P., Fierli, F., Mallet, M., and Ravetta, F.: Continental pollution in the Western Mediterranean basin: large  
584 variability of the aerosol single scattering albedo and influence on the direct shortwave radiative effect, *Atmos.*  
585 *Chem. Phys.*, 16, 10591–10607, <https://doi.org/10.5194/acp-16-10591-2016>, 2016.

586 Drugé, T., Nabat, P., Mallet, M., and Somot, S.: Model simulation of ammonium and nitrate aerosols distribution  
587 in the Euro-Mediterranean region and their radiative and climatic effects over 1979–2016, *Atmos. Chem. Phys.*,  
588 19, 3707–3731, <https://doi.org/10.5194/acp-19-3707-2019>, 2019.

589 Dubovik, O., Sinyuk, A., Lapyonok, T., Holben, B. N., Mishchenko, M., Yang, P., Eck, T. F., Volten, H., Muñoz,  
590 O., Veißelmann, B., van der Zande, W. J., Leon, J.-F., Sorokin, M., and Slutsker, I.: Application of spheroid  
591 models to account for aerosol particle nonsphericity in remote sensing of desert dust, *J. Geophys. Res.*, 111,  
592 D11208, <https://doi.org/10.1029/2005JD006619>, 2006.

593 Dulac, F., Tanré, D., Bergametti, G., Buat-Ménard, P., Desbois, M., and Sutton, D.: Assessment of the African  
594 airborne dust mass over the western Mediterranean Sea using Meteosat data, *J. Geophys. Res.*, 97, 2489–2506,  
595 <https://doi.org/10.1029/91JD02427>, 1992.

596 Floutsi, A.A., M.B. Korras-Carraca, C. Matsoukas, N. Hatzianastassiou, and G. Biskos, *Climatology and trends*  
597 *of aerosol optical depth over the Mediterranean basin during the last 12 years (2002-2014) based on Collection*  
598 *006 MODIS-Aqua data*, *Sci. Total Environ.*, 551–552, 292–293, <https://doi.org/10.1016/j.scitotenv.2016.01.192>,  
599 2016.

600 Formenti, P. (Coord.), *Mediterranean aerosol properties, Part VII in: Mediterranean Atmospheric Chemistry in the*  
601 *Mediterranean – Vol. 2, From Pollutant Sources to Impacts*, Dulac, F., Sauvage, S., and Eric Hamonou (Eds.),  
602 Springer, in prep., 2020.

603 Formenti, P., Mbemba Kabuiku, L., Chiapello, I., Ducos, F., Dulac, F., and Tanré, D.: Aerosol optical properties  
604 derived from POLDER-3/PARASOL (2005–2013) over the western Mediterranean Sea – Part 1: Quality  
605 assessment with AERONET and in situ airborne observations, *Atmos. Meas. Tech.*, 11, 6761–6784,  
606 <https://doi.org/10.5194/amt-11-6761-2018>, 2018.

607 Fougnie, B., Improvement of the PARASOL Radiometric In-Flight Calibration Based on Synergy Between  
608 Various Methods Using Natural Targets, in *IEEE Transactions on Geoscience and Remote Sensing*, vol. 54, no.  
609 4, pp. 2140-2152, April 2016, doi: 10.1109/TGRS.2015.2496322, 2016.

610 Georgoulas, A. K., Alexandri, G., Kourtidis, K. A., Lelieveld, J., Zanis, P., Pöschl, U., Levy, R., Amiridis, V.,  
611 Marinou, E., and Tsikerdekis, A.: Spatiotemporal variability and contribution of different aerosol types to the  
612 aerosol optical depth over the Eastern Mediterranean, *Atmos. Chem. Phys.*, 16, 13853–13884,  
613 <https://doi.org/10.5194/acp-16-13853-2016>, 2016.

614 Gkikas, A., Basart, S., Hatzianastassiou, N., Marinou, E., Amiridis, V., Kazadzis, S., Pey, J., Querol, X., Jorba,  
615 O., Gassó, S., and Baldasano, J. M.: Mediterranean intense desert dust outbreaks and their vertical structure based  
616 on remote sensing data, *Atmos. Chem. Phys.*, 16, 8609–8642, <https://doi.org/10.5194/acp-16-8609-2016>, 2016.

617 Gkikas, A., Hatzianastassiou, N., Mihalopoulos, N., Katsoulis, V., Kazadzis, S., Pey, J., Querol, X., and Torres,  
618 O.: The regime of intense desert dust episodes in the Mediterranean based on contemporary satellite observations  
619 and ground measurements, *Atmos. Chem. Phys.*, 13, 12135–12154, <https://doi.org/10.5194/acp-13-12135-2013>,  
620 2013.

621 Hansson, H.-C.; Tunved, P.; Krejci, R.; Freud, E.; Kalivitis, N.; Hennig, T.; Maneas, G.; Gerasopoulos, E. The  
622 Atmospheric Aerosol over Western Greece-Six Years of Aerosol Observations at the Navarino Environmental  
623 Observatory. *Atmosphere*, 12, 445. <https://doi.org/10.3390/atmos12040445>, 2021.

624 Hatzianastassiou, N., A. Gkikas, N. Mihalopoulos, O. Torres, and B. D. Katsoulis (2009), Natural versus  
625 anthropogenic aerosols in the eastern Mediterranean basin derived from multiyear TOMS and MODIS satellite  
626 data, *J. Geophys. Res.*, 114, D24202, <https://doi.org/10.1029/2009JD011982>.

627 Herman, M., Deuzé, J. L., Marchand, A., Roger, B., and Lallart, P.: Aerosol remote sensing from  
628 POLDER/ADEOS over the ocean: Improved retrieval using a nonspherical particle model, *J. Geophys. Res.*, 110,  
629 D10S02, <https://doi.org/10.1029/2004JD004798>, 2005.

630 Holben, B. N., Tanré, D., Smirnov, A., Eck, T. F., Slutsker, I., Abuhassan, N., Newcomb, W. W., Schafer, J. S.,  
631 Chatenet, B., Lavenue, F., Kaufman, Y. J., Castle, J. Vande, Setzer, A., Markham, B., Clark, D., Frouin, R.,  
632 Halthore, R., Karneli, A., O'Neill, N. T., Pietras, C., Pinker, R. T., Voss, K., and Zibordi, G.: An emerging ground-  
633 based aerosol climatology: Aerosol optical depth from AERONET, *J. Geophys. Res. Atmos.*, 106, 12067–12097,  
634 <https://doi.org/10.1029/2001JD900014>, 2001.

635 Hurrell, J. W., Decadal trend in the North Atlantic Oscillation: Regional temperatures and precipitations, *Science*,  
636 269, 676–679, <https://doi.org/10.1126/science.269.5224.676>, 1995.

637 Kaskaoutis D. G., Shailesh Kumar Kharol, N. Sifakis, P.T. Nastos, Anu Rani Sharma, K.V.S. Badarinath, H.D.  
638 Kambezidis, Satellite monitoring of the biomass-burning aerosols during the wildfires of August 2007 in Greece:  
639 Climate implications, *Atmospheric Environment*, Volume 45, Issue 3, Pages 716-726,  
640 <https://doi.org/10.1016/j.atmosenv.2010.09.043>, 2011.

641 Laj, P., Klausen, J., Bilde, M., Plass-Duelmer, C., Pappalardo, G., Clerbaux, C., Baltensperger, U., Hjorth, J.,  
642 Simpson, D., Reimann, S. and Coheur, P. F.: Measuring atmospheric composition change, *Atmos. Environ.*, 43,  
643 5351–5414, <https://doi.org/10.1016/j.atmosenv.2009.08.020>, 2009.

644 Laj, P., Bigi, A., Rose, C., Andrews, E., Lund Myhre, C., Collaud Coen, M., Lin, Y., Wiedensohler, A., Schulz,  
645 M., Ogren, J. A., Fiebig, M., Gliß, J., Mortier, A., Pandolfi, M., Petäjä, T., Kim, S.-W., Aas, W., Putaud, J.-P.,  
646 Mayol-Bracero, O., Keywood, M., Labrador, L., Aalto, P., Ahlberg, E., Alados Arboledas, L., Alastuey, A.,



647 Andrade, M., Artiñano, B., Ausmeel, S., Arsov, T., Asmi, E., Backman, J., Baltensperger, U., Bastian, S., Bath,  
648 O., Beukes, J. P., Brem, B. T., Bukowiecki, N., Conil, S., Couret, C., Day, D., Dayantolis, W., Degorska, A.,  
649 Eleftheriadis, K., Fetfatzis, P., Favez, O., Flentje, H., Gini, M. I., Gregorič, A., Gysel-Beer, M., Hallar, A. G.,  
650 Hand, J., Hoffer, A., Hueglin, C., Hooda, R. K., Hyvärinen, A., Kalapov, I., Kalivitis, N., Kasper-Giebl, A., Kim,  
651 J. E., Kouvarakis, G., Kranjc, I., Krejci, R., Kulmala, M., Labuschagne, C., Lee, H.-J., Lihavainen, H., Lin, N.-H.,  
652 Löschau, G., Luoma, K., Marinoni, A., Martins Dos Santos, S., Meinhardt, F., Merkel, M., Metzger, J.-M.,  
653 Mihalopoulos, N., Nguyen, N. A., Ondracek, J., Pérez, N., Perrone, M. R., Petit, J.-E., Picard, D., Pichon, J.-M.,  
654 Pont, V., Prats, N., Prenni, A., Reisen, F., Romano, S., Sellegri, K., Sharma, S., Schauer, G., Sheridan, P., Sherman,  
655 J. P., Schütze, M., Schwerin, A., Sohmer, R., Sorribas, M., Steinbacher, M., Sun, J., Titos, G., Toczko, B., Tuch,  
656 T., Tulet, P., Tunved, P., Vakkari, V., Velarde, F., Velasquez, P., Villani, P., Vratolis, S., Wang, S.-H., Weinhold,  
657 K., Weller, R., Yela, M., Yus-Diez, J., Zdimal, V., Zieger, P., and Zikova, N.: A global analysis of climate-relevant  
658 aerosol properties retrieved from the network of Global Atmosphere Watch (GAW) near-surface observatories,  
659 *Atmos. Meas. Tech.*, 13, 4353–4392, <https://doi.org/10.5194/amt-13-4353-2020>, 2020.

660 Lelieveld, J., Berresheim, H., Borrmann, S., Crutzen, P. J., Dentener, F. J., Fischer, H., Feichter, J., Flatau, P. J.,  
661 Heland, J., Holzinger, R., Kormann, R., Lawrence, M. G., Levin, Z., Markowicz, K. M., Mihalopoulos, N.,  
662 Minikin, a, Ramanathan, V., De Reus, M., Roelofs, G. J., Scheeren, H. a, Sciare, J., Schlager, H., Schultz, M.,  
663 Siegmund, P., Steil, B., Stephanou, E. G., Stier, P., Traub, M., Warneke, C., Williams, J., and Ziereis, H.: Global  
664 air pollution crossroads over the Mediterranean, *Science*, 298, 794–9, <https://doi.org/10.1126/science.1075457>,  
665 2002.

666 Lyamani, H., Valenzuela, A., Perez-Ramirez, D., Toledano, C., Granados-Muñoz, M. J., Olmo, F. J., and Alados-  
667 Arboledas, L.: Aerosol properties over the western Mediterranean basin: temporal and spatial variability, *Atmos.*  
668 *Chem. Phys.*, 15, 2473–2486, <https://doi.org/10.5194/acp-15-2473-2015>, 2015.

669 Mallet, M., Dulac, F., Formenti, P., Nabat, P., Sciare, J., Roberts, G., Pelon, J., Ancellet, G., Tanré, D., Parol, F.,  
670 Denjean, C., Brogniez, G., di Sarra, A., Alados-Arboledas, L., Arndt, J., Auriol, F., Blarel, L., Bourrienne, T.,  
671 Chazette, P., Chevaillier, S., Claeys, M., D'Anna, B., Derimian, Y., Desboeufs, K., Di Iorio, T., Doussin, J.-F.,  
672 Durand, P., Féron, A., Freney, E., Gaimoz, C., Goloub, P., Gómez-Amo, J. L., Granados-Muñoz, M. J., Grand,  
673 N., Hamonou, E., Jankowiak, I., Jeannot, M., Léon, J.-F., Maillé, M., Mailler, S., Meloni, D., Menut, L.,  
674 Momboisse, G., Nicolas, J., Podvin, T., Pont, V., Rea, G., Renard, J.-B., Roblou, L., Schepanski, K.,  
675 Schwarzenboeck, A., Sellegri, K., Sicard, M., Solmon, F., Somot, S., Torres, B., Totems, J., Triquet, S., Verdier,  
676 N., Verwaerde, C., Waquet, F., Wenger, J., and Zapf, P.: Overview of the Chemistry-Aerosol Mediterranean  
677 Experiment/Aerosol Direct Radiative Forcing on the Mediterranean Climate (ChArMEx/ADRMED) summer  
678 2013 campaign, *Atmos. Chem. Phys.*, 16, 455-504, <https://doi.org/10.5194/acp-16-455-2016>, 2016.

679 Menut, L., Siour, G., Mailler, S., Couvidat, F., and Bessagnet, B.: Observations and regional modeling of aerosol  
680 optical properties, speciation and size distribution over northern Africa and western Europe, *Atmos. Chem. Phys.*,  
681 16, 12961–12982, <https://doi.org/10.5194/acp-16-12961-2016>, 2016.

682 Michoud, V., Sciare, J., Sauvage, S., Dusanter, S., Léonardis, T., Gros, V., Kalogridis, C., Zannoni, N., Féron, A.,  
683 Petit, J.-E., Crenn, V., Baisnée, D., Sarda-Estève, R., Bonnaire, N., Marchand, N., DeWitt, H. L., Pey, J., Colomb,  
684 A., Gheusi, F., Szidat, S., Stavroulas, I., Borbon, A., and Locoge, N.: Organic carbon at a remote site of the western  
685 Mediterranean Basin: composition, sources and chemistry during the ChArMEx SOP2 field experiment, *Atmos.*  
686 *Chem. Phys.*, 17, 8837–8865, <https://doi.org/10.5194/acp-17-8837-2017>, 2017.

687 Moulin, C., Lambert, C. E., Dayan, U., Masson, V., Ramonet, M., Bousquet, P., Legrand, M., Balkanski, Y. J.,  
688 Guelle, W., Marticorena, B., Bergametti, G., and Dulac, F.: Satellite climatology of African dust transport in the  
689 Mediterranean atmosphere, *J. Geophys. Res.*, 103, 13137, doi:10.1029/98JD00171, 1998.

690 Moulin, C., Lambert, C. E., Dulac, F., and Dayan, U.: Control of atmospheric export of dust from North Africa by  
691 the North Atlantic Oscillation, *Nature*, 387, 691–694, <https://doi.org/10.1038/42679>, 1997.

692 Nabat, P., Somot, S., Cassou, C., Mallet, M., Michou, M., Bouniol, D., Decharme, B., Drugé, T., Roehrig, R., and  
693 Saint-Martin, D.: Modulation of radiative aerosols effects by atmospheric circulation over the Euro-Mediterranean  
694 region, *Atmos. Chem. Phys.*, 20, 8315–8349, <https://doi.org/10.5194/acp-20-8315-2020>, 2020.

695 Nabat, P., Somot, S., Mallet, M., Chiapello, I., Morcrette, J. J., Solmon, F., Szopa, S., Dulac, F., Collins, W., Ghan,  
696 S., Horowitz, L. W., Lamarque, J. F., Lee, Y. H., Naik, V., Nagashima, T., Shindell, D., and Skeie, R.: A 4-D  
697 climatology (1979-2009) of the monthly tropospheric aerosol optical depth distribution over the Mediterranean  
698 region from a comparative evaluation and blending of remote sensing and model products, *Atmos. Meas. Tech.*,  
699 6, 1287–1314, doi:10.5194/amt-6-1287-2013, 2013.

700 Pandolfi, M., Alastuey, A., Pérez, N., Reche, C., Castro, I., Shatalov, V., and Querol, X.: Trends analysis of PM  
701 source contributions and chemical tracers in NE Spain during 2004–2014: a multi-exponential approach, *Atmos.*  
702 *Chem. Phys.*, 16, 11787–11805, <https://doi.org/10.5194/acp-16-11787-2016>, 2016.

703 Pandolfi, M., Alados-Arboledas, L., Alastuey, A., Andrade, M., Angelov, C., Artiñano, B., Backman, J.,  
704 Baltensperger, U., Bonasoni, P., Bukowiecki, N., Collaud Coen, M., Conil, S., Coz, E., Crenn, V., Dudoitis, V.,  
705 Ealo, M., Eleftheriadis, K., Favez, O., Fetfatzis, P., Fiebig, M., Flentje, H., Ginot, P., Gysel, M., Henzing, B.,  
706 Hoffer, A., Holubova Smejkalova, A., Kalapov, I., Kalivitis, N., Kouvarakis, G., Kristensson, A., Kulmala, M.,  
707 Lihavainen, H., Lunder, C., Luoma, K., Lyamani, H., Marinoni, A., Mihalopoulos, N., Moerman, M., Nicolas, J.,  
708 O'Dowd, C., Petäjä, T., Petit, J.-E., Pichon, J. M., Prokopciuk, N., Putaud, J.-P., Rodríguez, S., Sciare, J., Sellegri,  
709 K., Swietlicki, E., Titos, G., Tuch, T., Tunved, P., Ulevicius, V., Vaishya, A., Vana, M., Virkkula, A., Vratolis,  
710 S., Weingartner, E., Wiedensohler, A., and Laj, P.: A European aerosol phenomenology – 6: scattering properties  
711 of atmospheric aerosol particles from 28 ACTRIS sites, *Atmos. Chem. Phys.*, 18, 7877–7911,  
712 <https://doi.org/10.5194/acp-18-7877-2018>, 2018.

713 Papadimas, C. D., Hatzianastassiou, N., Mihalopoulos, N., Querol, X., and Vardavas, I.: Spatial and temporal  
714 variability in aerosol properties over the Mediterranean basin based on 6- year (2000–2006) MODIS data: *J.*  
715 *Geophys. Res.*, 113, D11205, <https://doi.org/10.1029/2007JD009189>, 2008.

716 Querol X., Alastuey A., Pandolfi M., Reche C., Pérez N., Minguillón M.C., Moreno T., Viana M., Escudero M.,  
717 Orio A., Pallarés M., Reina F.: 2001-2012 trends on air quality in Spain, *Sci Total Environ.*, Aug 15;490:957-69.  
718 doi: 10.1016/j.scitotenv.2014.05.074.2014.

719 Rea, G., Turquety, S., Menut, L., Briant, R., Mailler, S., and Siour, G.: Source contributions to 2012 summertime  
720 aerosols in the Euro-Mediterranean region, *Atmos. Chem. Phys.*, 15, 8013–8036, doi:10.5194/acp-15-8013-2015,  
721 2015.

722 Remer, L.R., R. C. Levy, S. Mattoo, D. Tanré, P. Gupta, Y. Shi, V. Sawyer, L. A. Munchak, Y. Zhou, M. Kim, C.  
723 Ichoku, F. Patadia, R.-R. Li, S. Gassó, R. G. Kleidman, and B. N. Holben, The Dark Target Algorithm for  
724 Observing the Global Aerosol System: Past, Present, and Future, *Remote Sens.* 2020, 12, 2900 ;  
725 doi :10.3390/rs12182900,2020.

726 Ricaud, P., Zbinden, R., Catoire, V., Brocchi, V., Dulac, F., Hamonou, E., Canonici, J.-C., El Amraoui, L.,

727 Massart, S., Pignatelli, B., Dayan, U., Nabat, P., Sciare, J., Ramonet, M., Delmotte, M., di Sarra, A., Sferlazzo, D.,  
728 di Iorio, T., Piacentino, S., Cristofanelli, P., Mihalopoulos, N., Kouvarakis, G., Pikridas, M., Savvides, C.,  
729 Mamouri, R.-E., Nisantzi, A., Hadjimitsis, D., Attié, J.-L., Ferré, H., Kangah, Y., Jaidan, N., Guth, J., Jacquet, P.,  
730 Chevrier, S., Robert, C., Bourdon, A., Bourdinot, J.-F., Etienne, J.-C., Krysztofiak, G., and Théron, P.: The GLAM  
731 airborne campaign across the Mediterranean basin, *Bull. Am. Met. Soc.*, 99, 361–380,  
732 <https://doi.org/10.1175/BAMS-D-16-0226.1>, 2018.

733 Salvador, P., Alonso-Pérez, S., Pey, J., Artíñano, B., de Bustos, J. J., Alastuey, A., and Querol, X.: African dust  
734 outbreaks over the western Mediterranean Basin: 11-year characterization of atmospheric circulation patterns and  
735 dust source areas, *Atmos. Chem. Phys.*, 14, 6759–6775, <https://doi.org/10.5194/acp-14-6759-2014>, 2014.

736 Shaheen, A., Wu, R., Aldabash, M., Long-term AOD trend assessment over the Eastern Mediterranean region: A  
737 comparative study including a new merged aerosol product, *Atmosph. Environm.*, 238, 117736,  
738 <https://doi.org/10.1016/j.atmosenv.2020.117736>, 2020.

739 Sič, B., El Amraoui, L., Piacentini, A., Marécal, V., Emili, E., Cariolle, D., Prather, M., and Attié, J.-L.: Aerosol  
740 data assimilation in the chemical-transport model MOCAGE during the TRAQA/ChArMEx campaign: Aerosol  
741 optical depth, *Atmos. Meas. Tech.*, 9, 5535–5554, <https://doi.org/10.5194/amt-9-5535-2016>, 2016.

742 Sicard, M., R. Barragan, F. Dulac, L. Alados-Arboledas, and M. Mallet : Aerosol optical, microphysical and  
743 radiative properties at regional background insular sites in the western Mediterranean, *Atmos. Chem. Phys.*, 16,  
744 12177–12203, <https://doi.org/10.5194/acp-16-12177-2016>, 2016.

745 Tanré, D., Bréon, F. M., Deuzé, J. L., Dubovik, O., Ducos, F., François, P., Goloub, P., Herman, M., Lifermann,  
746 A. and Waquet, F.: Remote sensing of aerosols by using polarized, directional and spectral measurements within  
747 the A-Train: the PARASOL mission, *Atmos. Meas. Tech.*, 4, 1383–1395, [https://doi.org/10.5194/amt-4-1383-](https://doi.org/10.5194/amt-4-1383-2011)  
748 [2011](https://doi.org/10.5194/amt-4-1383-2011), 2011.

749  
750  
751  
752  
753  
754  
755  
756  
757  
758  
759  
760  
761  
762  
763  
764  
765  
766  
767  
768  
769  
770

771  
772  
773

	AOD			AE			AOD <sub>F</sub>			AOD <sub>c</sub>		
	North	Central	South	North	Central	South	North	Central	South	North	Central	South
Winter (DJF)	0.062	0.064	0.074	0.950	0.792	0.723	0.025	0.022	0.021	0.037	0.042	0.058
Spring (MAM)	0.106	0.115	0.155	1.064	0.855	0.724	0.043	0.038	0.040	0.063	0.078	0.115
Summer (JJA)	0.106	0.126	0.153	0.947	0.819	0.737	0.038	0.038	0.040	0.068	0.088	0.113
Fall (SON)	0.079	0.086	0.104	0.963	0.831	0.734	0.033	0.030	0.031	0.047	0.057	0.074
<b>Annual</b>	<b>0.090</b>	<b>0.099</b>	<b>0.124</b>	<b>0.985</b>	<b>0.826</b>	<b>0.729</b>	<b>0.035</b>	<b>0.032</b>	<b>0.033</b>	<b>0.055</b>	<b>0.067</b>	<b>0.091</b>
	Fine Mode Fraction %			AOD <sub>CNS</sub>			AOD <sub>CS</sub>					
	North	Central	South	North	Central	South	North	Central	South			
Winter (DJF)	40	34	30	0.033	0.034	0.048	0.013	0.016	0.018			
Spring (MAM)	42	34	29	0.048	0.062	0.088	0.021	0.026	0.029			
Summer (JJA)	36	31	27	0.046	0.058	0.091	0.021	0.027	0.031			
Fall (SON)	40	35	30	0.041	0.047	0.059	0.015	0.019	0.023			
<b>Annual</b>	<b>40</b>	<b>33</b>	<b>29</b>	<b>0.043</b>	<b>0.051</b>	<b>0.073</b>	<b>0.018</b>	<b>0.022</b>	<b>0.026</b>			

774  
775  
776  
777  
778  
779  
780

**Table 1a.** The 8 (winter) or 9-year (March 2005 – October 2013) climatological seasonal averaged values of POLDER-3 advanced aerosol products at 865 nm for the north (NW MED), central (CW MED), and south (SW MED) parts of western Mediterranean basins (defined in Figure 2). Maximum values are reported in red, minimum, in blue.

	AOD			AOD <sub>F</sub>			AOD <sub>c</sub>			Fine Mode Fraction %		
	North	Central	South	North	Central	South	North	Central	South	North	Central	South
Winter (DJF)	0.099	0.093	0.106	0.069	0.059	0.058	0.030	0.035	0.049	65	60	56
Spring (MAM)	0.168	0.166	0.204	0.118	0.104	0.109	0.049	0.062	0.095	70	62	57
Summer (JJA)	0.163	0.180	0.208	0.110	0.110	0.117	0.053	0.070	0.091	66	61	57
Fall (SON)	0.126	0.128	0.144	0.089	0.082	0.084	0.037	0.046	0.060	66	61	57
<b>Annual</b>	<b>0.141</b>	<b>0.143</b>	<b>0.167</b>	<b>0.098</b>	<b>0.089</b>	<b>0.093</b>	<b>0.043</b>	<b>0.053</b>	<b>0.074</b>	<b>67</b>	<b>61</b>	<b>57</b>

781  
782  
783  
784  
785  
786  
787  
788  
789  
790  
791  
792  
793  
794  
795  
796  
797  
798  
799  
800  
801  
802  
803  
804  
805  
806  
807  
808

**Table 1b.** Same as Table 1a for AOD, AOD<sub>F</sub>, AOD<sub>c</sub>, and Fine Mode Fraction at 550 nm for the north (NW MED), central (CW MED), and south (SW MED) parts of western Mediterranean basins (defined in Figure 2). Maximum values are reported in red, minimum, in blue.

809  
810  
811  
812  
813

	Ersa N <sub>ACSP</sub> = 1242 - N <sub>BVC</sub> = 556		Barcelona N <sub>ACSP</sub> = 1241 - N <sub>BVC</sub> = 540		Lampedusa N <sub>ACSP</sub> = 1320 - N <sub>BVC</sub> = 612	
	Mean ± SD	Range Min – Max	Mean ± SD	Range Min – Max	Mean ± SD	Range Min – Max
ACSP AOD <sub>865 nm</sub>	0.09 ± 0.07	0.01 – 0.68	0.10 ± 0.04	0.01 – 1.05	0.15 ± 0.18	0.02 – 4.72
ACSP AOD <sub>F 865 nm</sub>	0.03 ± 0.03	<0.01 – 0.16	0.04 ± 0.03	<0.01 – 0.19	0.04 ± 0.03	<0.01 – 0.35
ACSP AOD <sub>C 865 nm</sub>	0.06 ± 0.06	<0.01 – 0.65	0.07 ± 0.07	<0.01 – 0.94	0.11 ± 0.16	<0.01 – 4.37
ACSP AE <sub>865-670</sub>	0.94 ± 0.53	0.01 – 2.23	0.90 ± 0.50	-0.07 – 2.33	0.67 ± 0.42	0.00 – 2.24
ACSP FMF (%)	38 ± 23	3 – 100	37 ± 22	1 – 97	28 ± 18	3 – 100
BVC AOD <sub>CNS 865nm</sub>	0.04 ± 0.04	<0.01 – 0.48	0.05 ± 0.05	<0.01 – 0.42	0.08 ± 0.09	<0.01 – 1.00
BVC AOD <sub>CS 865nm</sub>	0.02 ± 0.03	<0.01 – 0.24	0.02 ± 0.03	<0.01 – 0.34	0.03 ± 0.03	<0.01 – 0.33

814  
815  
816  
817  
818  
819  
820  
821  
822  
823  
824  
825  
826  
827  
828  
829  
830  
831  
832  
833  
834  
835  
836  
837  
838  
839  
840  
841  
842  
843  
844  
845

**Table 2.** Statistics of POLDER-3 daily retrievals of AOD, AOD<sub>F</sub>, AOD<sub>C</sub>, AE, FMF (Fine Mode Fraction), AOD<sub>CS</sub>, and AOD<sub>CNS</sub> at three main stations, Ersu, Barcelona, and Lampedusa for the period March 2005 - October 2013. The numbers of POLDER-3 retrievals available at each station for all clear sky pixels (ACSP) and for best viewing conditions (BVC) are reported.

846  
847  
848  
849  
850  
851  
852  
853  
854

Trend per year Region	AOD 865 nm		AOD <sub>COARSE</sub> 865 nm		AOD <sub>FINE</sub> 865 nm	
	Annual means	Monthly anomalies	Annual means	Monthly anomalies	Annual means	Monthly anomalies
NW MED	<b>- 0.0030 ± 0.0011*</b>	<b>- 0.0031 ± 0.0006**</b>	- 0.0010 ± 0.0009	<b>- 0.0012 ± 0.0005*</b>	<b>- 0.0020 ± 0.0005**</b>	<b>- 0.0019 ± 0.0003**</b>
CW MED	<b>- 0.0035 ± 0.0010*</b>	<b>- 0.0035 ± 0.0007**</b>	- 0.0015 ± 0.0009	<b>- 0.0016 ± 0.0006**</b>	<b>- 0.0020 ± 0.0004**</b>	<b>- 0.0019 ± 0.0003**</b>
SW MED	- 0.0037 ± 0.0019	<b>- 0.0043 ± 0.0012**</b>	- 0.0021 ± 0.0016	<b>- 0.0027 ± 0.0010*</b>	<b>- 0.0016 ± 0.0004**</b>	<b>- 0.0016 ± 0.0003**</b>

855  
856  
857  
858  
859  
860  
861  
862  
863

**Table 3.** POLDER-3 865 nm AOD, AOD<sub>COARSE</sub> and AOD<sub>FINE</sub> trends per year derived from March-October annual means and monthly mean anomalies over the 2005-2013 period for NW MED, CW MED, SW MED. The corresponding annual evolutions are shown in Figure 9 and S6 (left columns). Trends (year<sup>-1</sup>) are shown with their standard deviations (± 1σ). Values in bold indicate statistically significant trends at \* 95% confidence level and \*\* 99% confidence level, as determined by the Student t-test.

Trend per year Station	AOD 865 nm		AOD <sub>COARSE</sub> 865 nm		AOD <sub>FINE</sub> 865 nm	
	Annual means	Monthly anomalies	Annual means	Monthly anomalies	Annual means	Monthly anomalies
Ersa	<b>- 0.0035 ± 0.0014*</b>	<b>- 0.0030 ± 0.0008**</b>	- 0.0012 ± 0.0012	- 0.0011 ± 0.0008	<b>- 0.0024 ± 0.0004**</b>	<b>- 0.0019 ± 0.0003**</b>
Barcelona	<b>- 0.0050 ± 0.0021*</b>	<b>- 0.0046 ± 0.0011**</b>	- 0.0021 ± 0.0017	<b>- 0.0020 ± 0.0009*</b>	<b>- 0.0029 ± 0.0005**</b>	<b>- 0.0026 ± 0.0004**</b>
Lampedusa	- 0.0037 ± 0.0028	- 0.0025 ± 0.0018	- 0.0021 ± 0.0026	- 0.0009 ± 0.0016	<b>- 0.0017 ± 0.0003**</b>	<b>- 0.0015 ± 0.0004**</b>

864  
865  
866  
867  
868  
869  
870  
871  
872  
873  
874  
875  
876

**Table 4.** POLDER-3 865 nm AOD, AOD<sub>COARSE</sub> and AOD<sub>FINE</sub> trends per year derived from March-October annual means and monthly mean anomalies over the 2005-2013 period for Ersa, Barcelona, and Lampedusa. The corresponding annual evolutions are shown in Figure 9 and S6 (right columns). Trends (year<sup>-1</sup>) are shown with their standard deviations (± 1σ). Values in bold indicate statistically significant trends at \* 95% confidence level and \*\* 99% confidence level, as determined by the Student t-test.

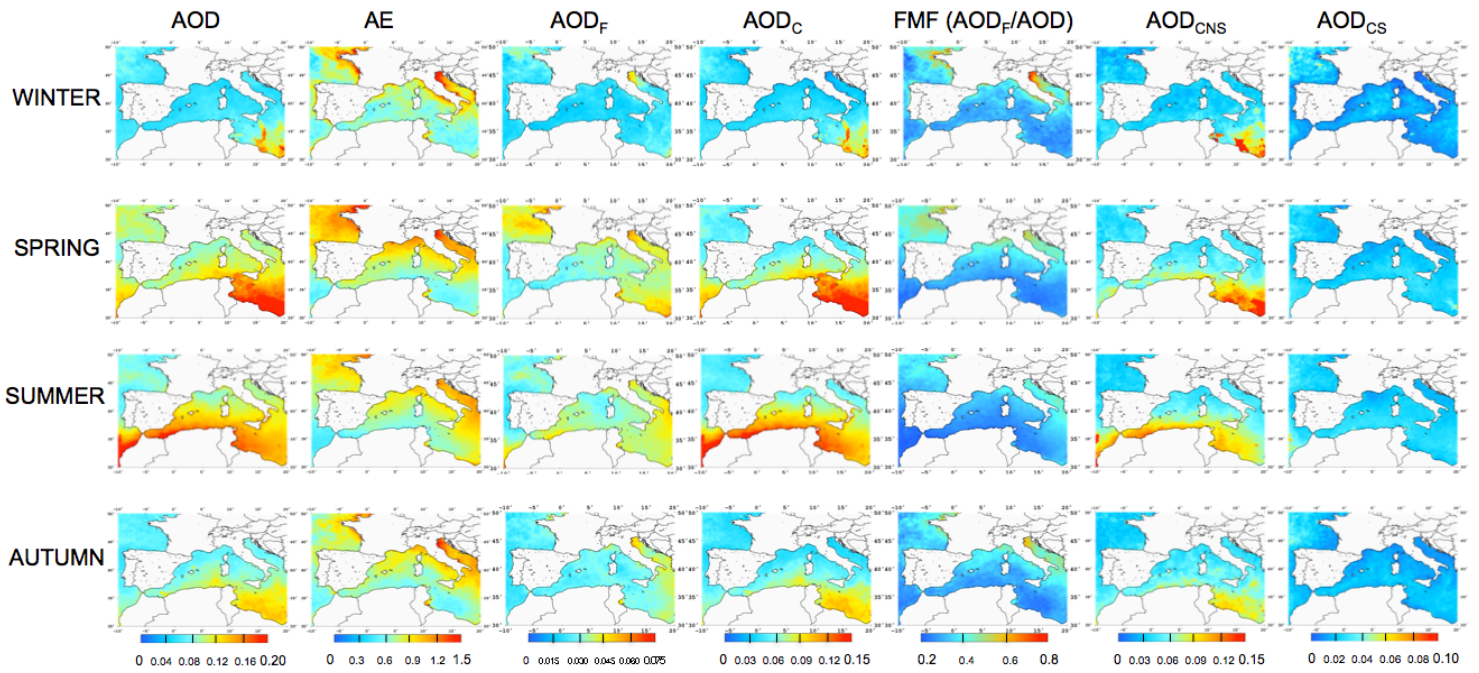


**Figure 1.** Climatological seasonal maps for AOD, AE, AOD<sub>F</sub>, AOD<sub>C</sub>, FMF (Fine Mode Fraction derived from AOD<sub>F</sub>/AOD), AOD<sub>CNS</sub>, and AOD<sub>CS</sub> retrieved by POLDER-3 at 865 nm over the period March 2005-October 2013. Seasons are ordered from the top to the bottom : Winter is December-January-February, Spring March-April-May, Summer June-July-August, Autumn September-October-November.

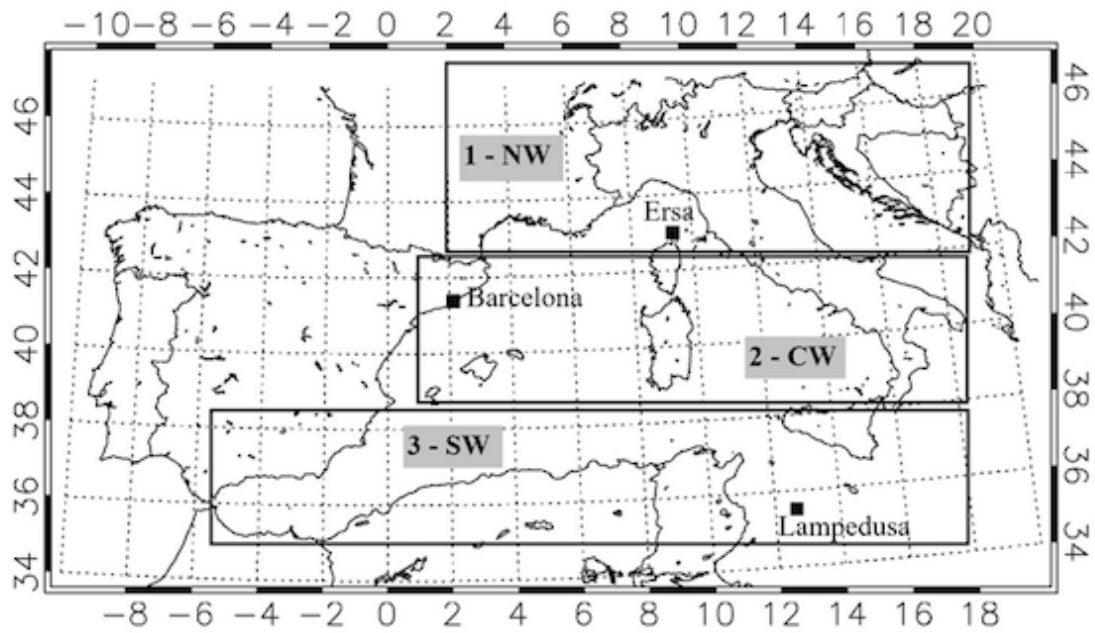


**Figure 2.** Definition of the three geographical sub-regions used to analyze POLDER-3 aerosol retrievals over the area of study: 1. NW Med, 42-46°N, 02°E-20°E – 2. CW MED, 38-42°N, 01°W-20°E, 3. SW MED, 34-38°N, 06°W-20°E. The three sites considered in this study are reported, i.e., Ersaa (43.00367°N, 09.35929°E), Barcelona (41.38925°N, 02.11206°E), and Lampedusa (35.51667°N, 12.63167°E).



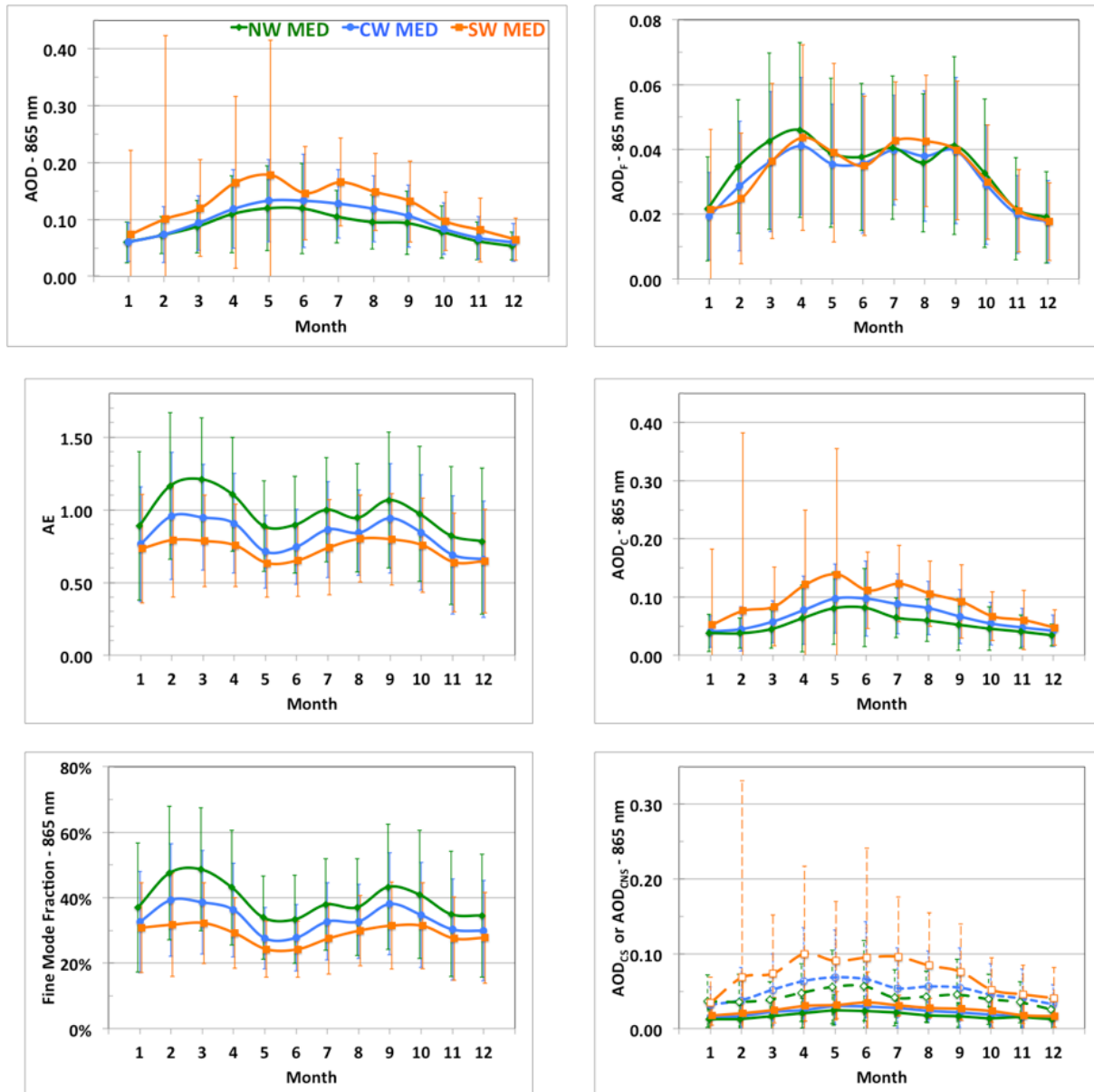


**Figure 3.** The 9-year (March 2005 – October 2013) climatological seasonal cycle of -Left column: AOD (top), Angström Exponent (middle), Fine Mode Fraction (bottom) – Right column: AOD<sub>Fine</sub> (top), AOD<sub>Coarse</sub> (middle), AOD<sub>Coarse Spherical</sub> (continuous lines) and AOD<sub>Coarse Non Spherical</sub> (dashed lines) (bottom), derived from POLDER-3 at 865 nm. The green, blue, orange curves are respectively for the north (NW MED), central (CW MED), and south (SW MED) parts of western Mediterranean basins (defined in Figure 2).

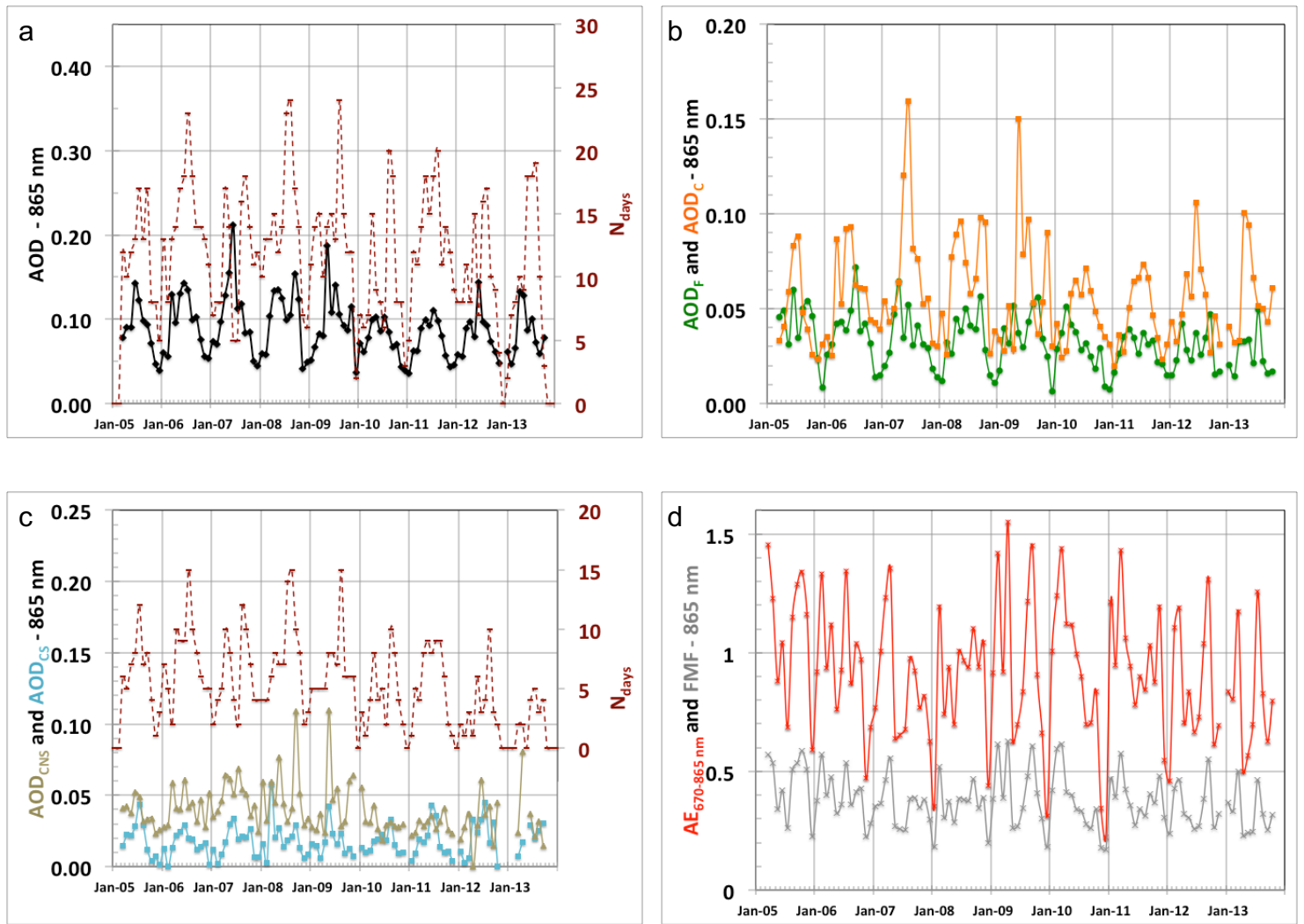


**Figure 4.** POLDER-3 monthly mean retrievals of (a) AOD, (b)  $AOD_F$  and  $AOD_C$ , (c)  $AOD_{CNS}$  and  $AOD_{CS}$ , (d)  $AE_{865-670}$  and FMF at 865 nm at Ersar over the period 2005-2013. The number of days of observations available for each month is reported for all clear days (right axis of Figure 4a), and for best viewing conditions (right axis of Figure 4c) necessary for retrievals of  $AOD_{CNS}$  and  $AOD_{CS}$ .

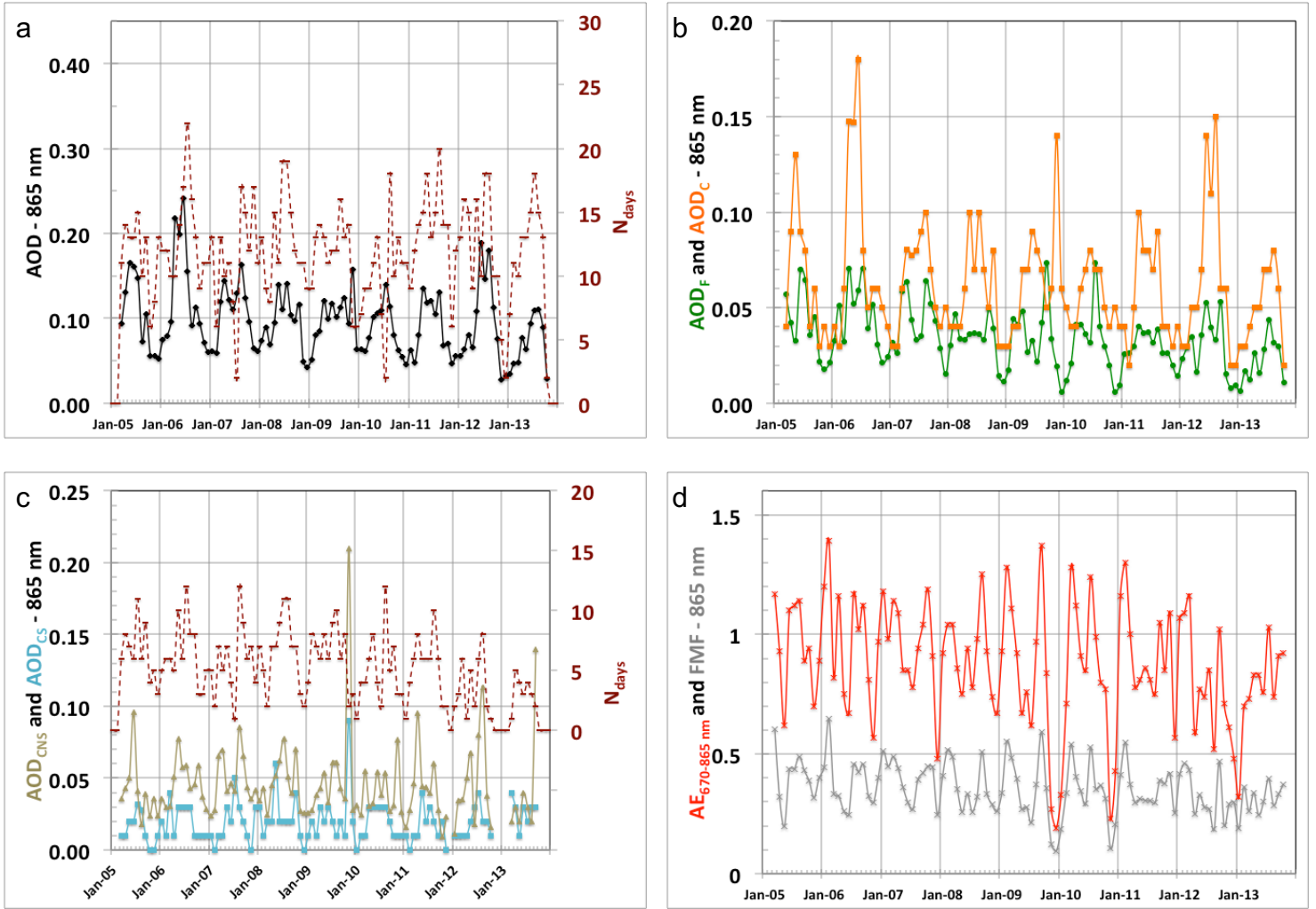
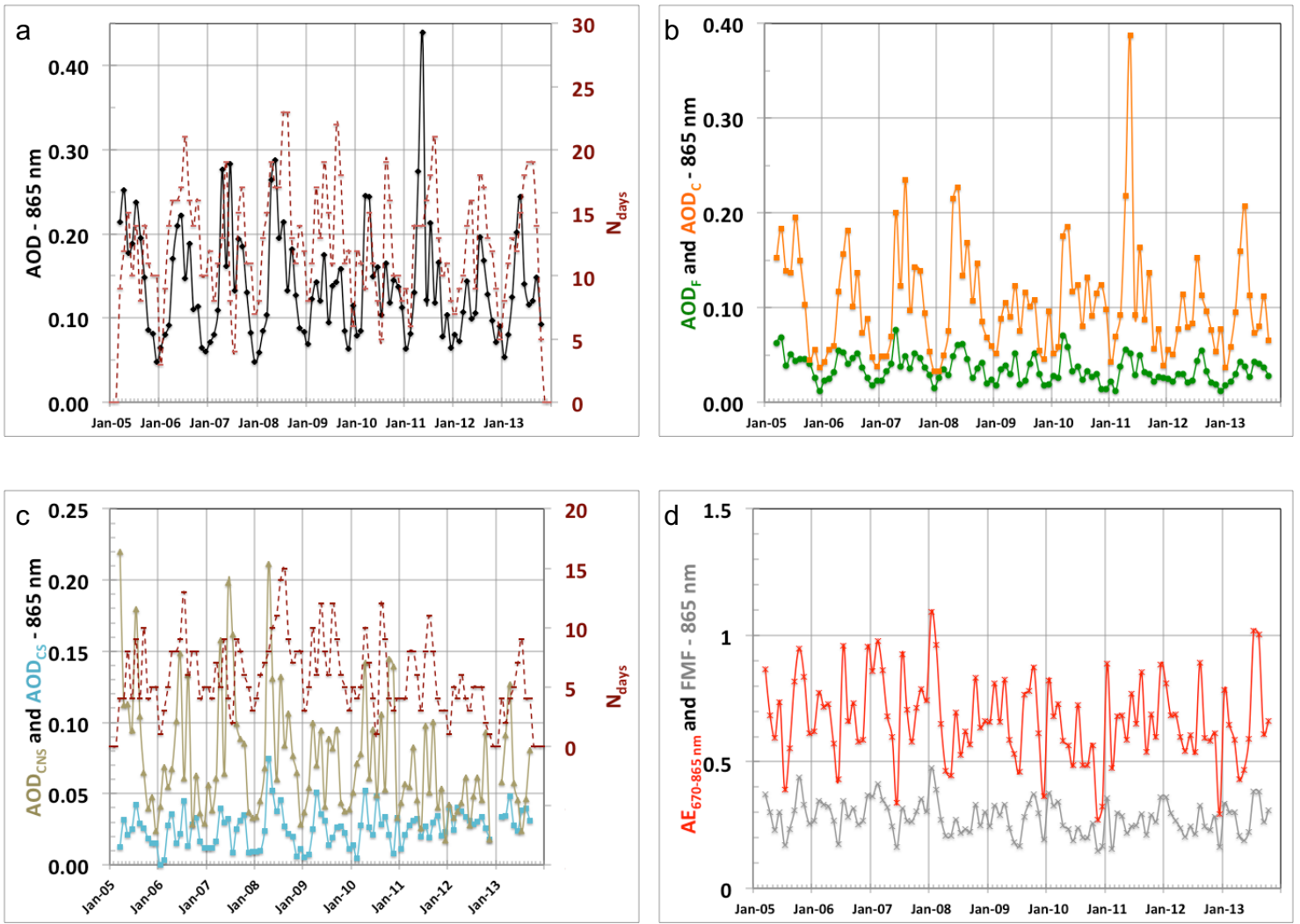
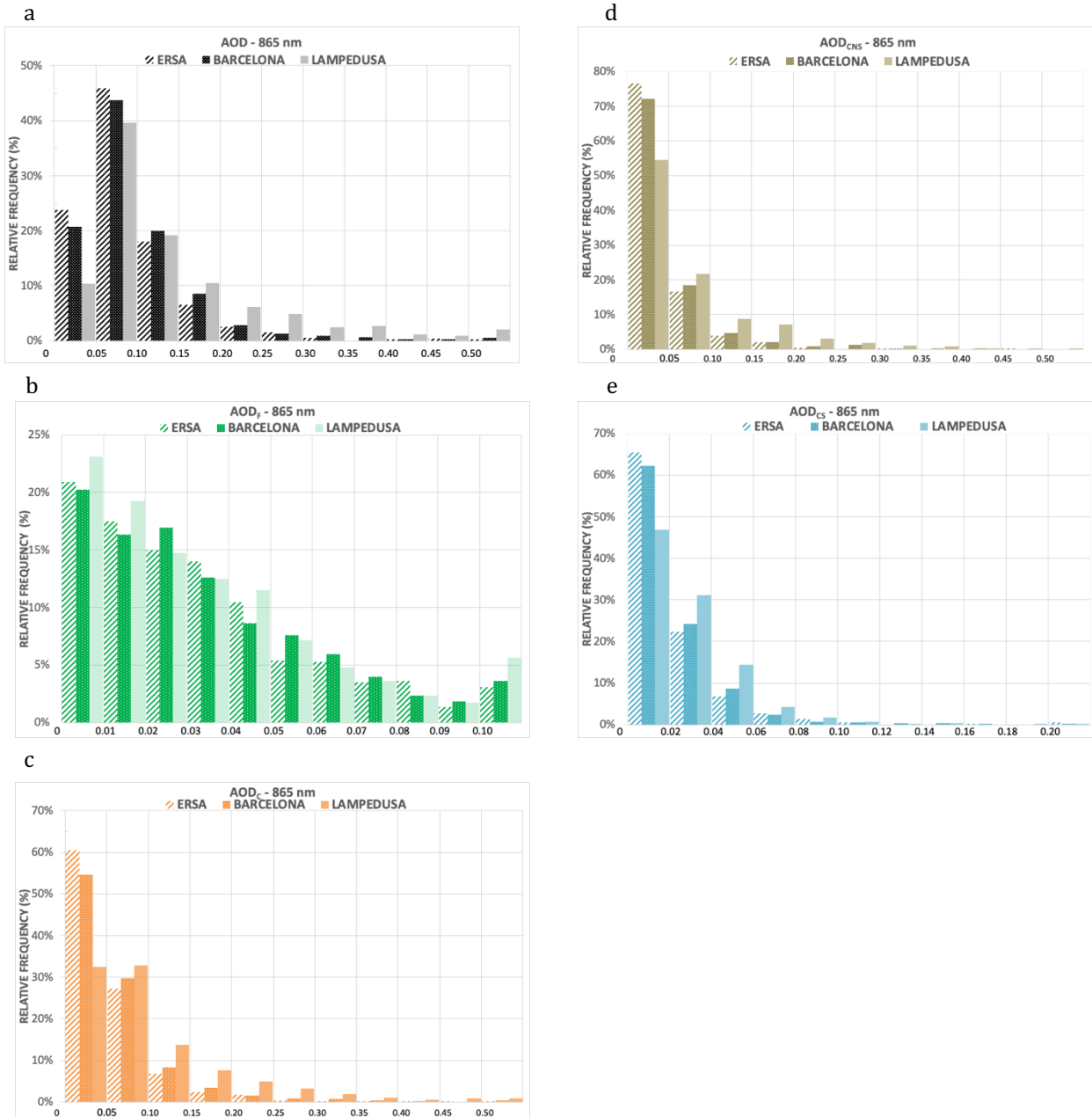


Figure 5. Same as Figure 4 for Barcelona.



**Figure 6.** Same as Figure 4 for Lampedusa. Note that the scale of Figure 6b is different from that of Figure 4b and 5b.



**Figure 7.** Frequency histograms for POLDER-3 daily retrievals at 865 nm of a- AOD, b- AOD<sub>F</sub>, c- AOD<sub>C</sub>, d- AOD<sub>CNS</sub>, e- AOD<sub>CS</sub> at Ersa, Barcelona, and Lampedusa.

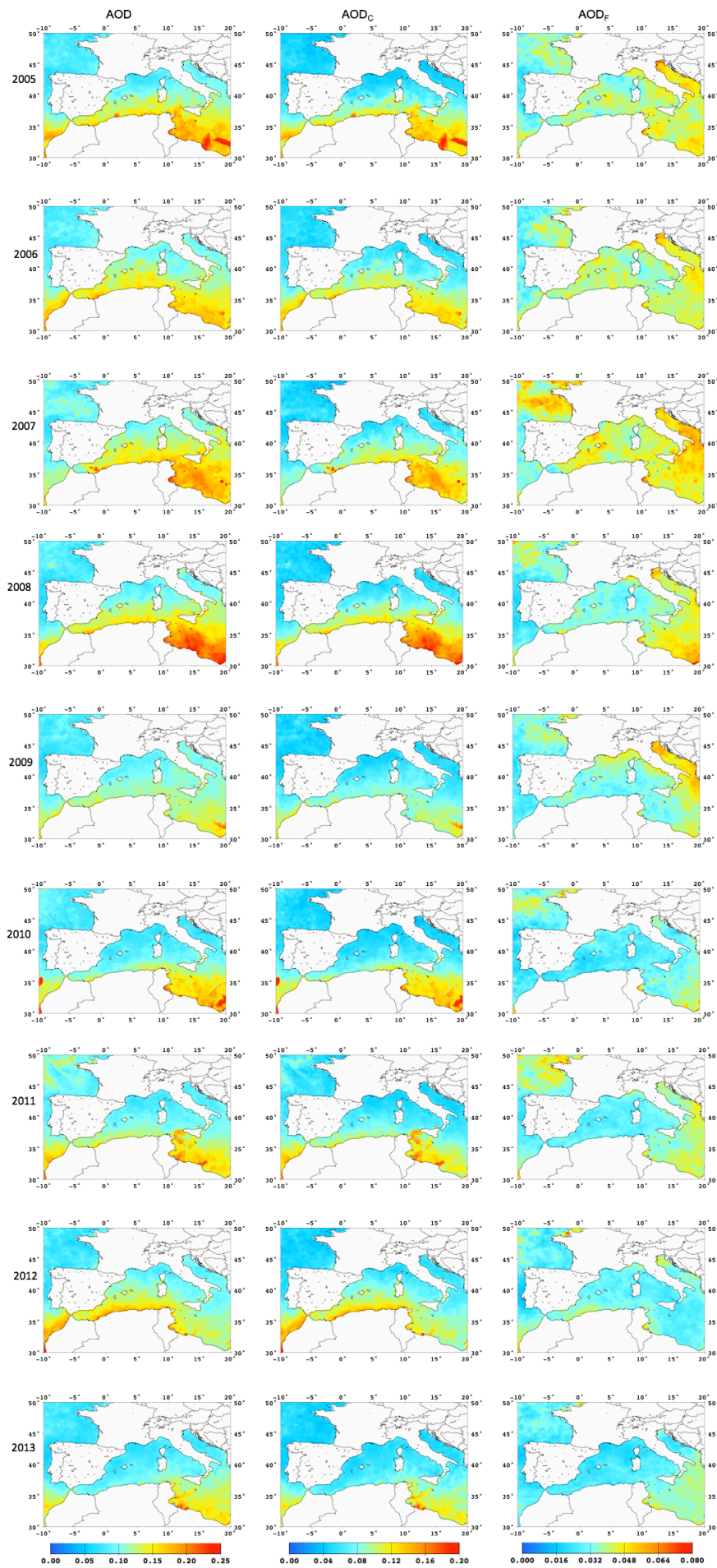


**Figure 8.** March-October annual averages of POLDER-3 AOD (left), AOD<sub>C</sub> (middle), AOD<sub>F</sub> (right) at 865 nm from 2005 to 2013.

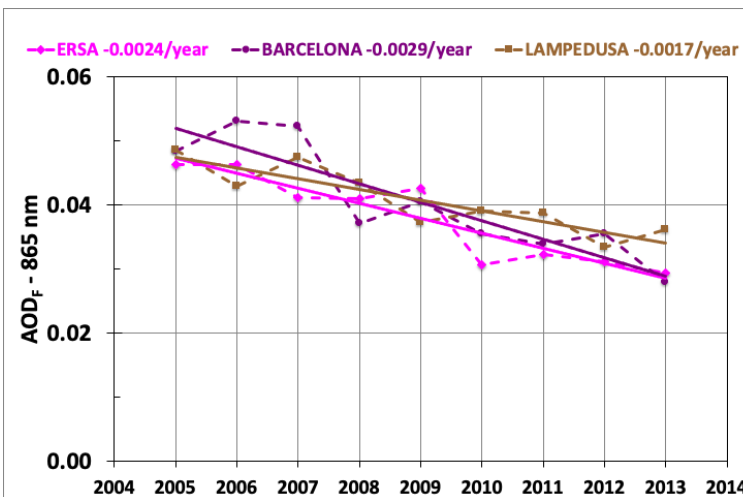
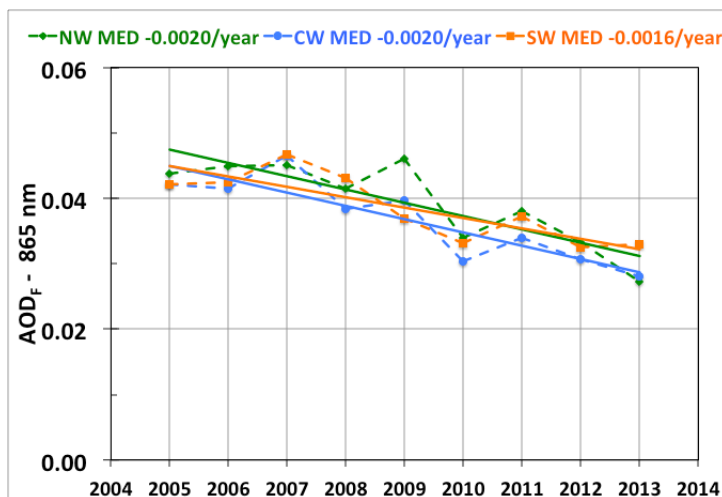
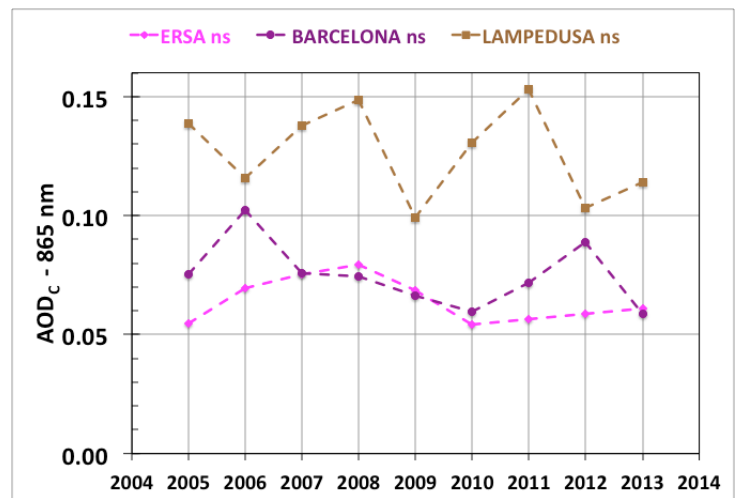
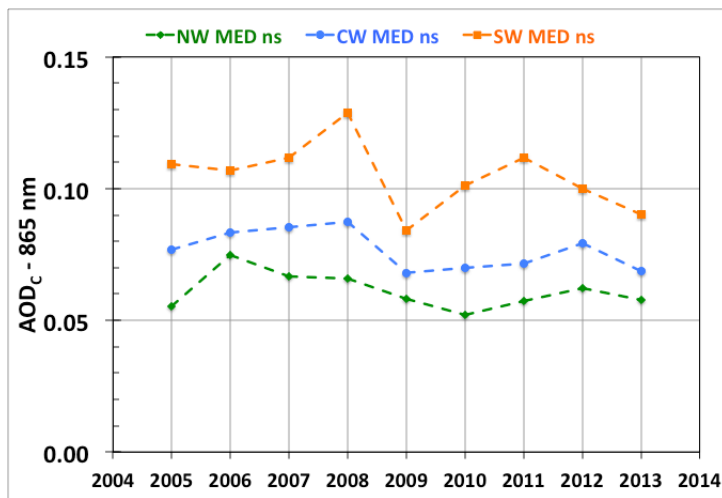
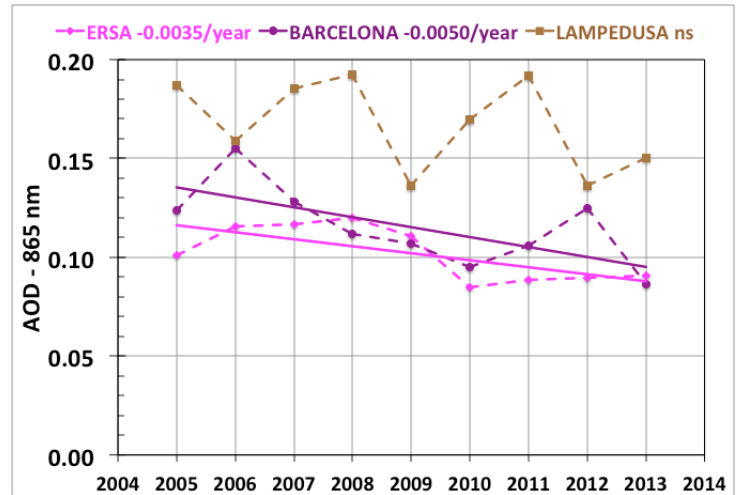
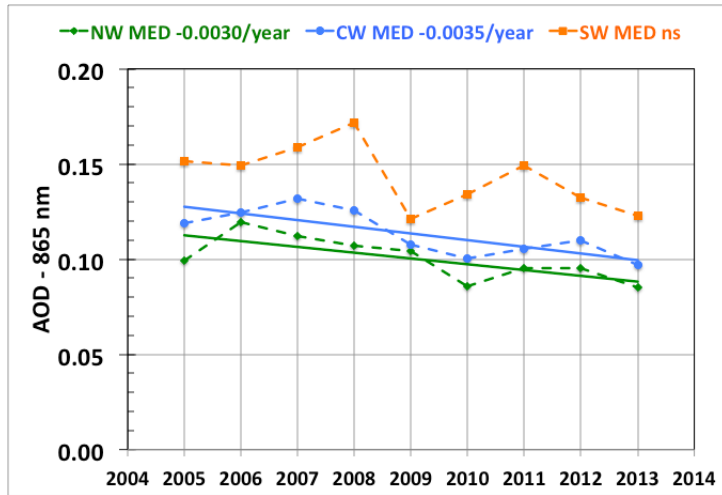


**Figure 9.** March to October yearly means of POLDER-3 retrievals at 865 nm over the period 2005–2013: AOD (top), AOD<sub>COARSE</sub> (middle), AOD<sub>FINE</sub> (bottom). In the left column, spatial averages over north (NW MED, green curves), central (CW MED, blue curves), and south (SW MED, orange curves) parts of western Mediterranean basins (defined Figure 2). In the right column, values extracted at Ersa (pink curves), Barcelona (purple curves), and Lampedusa (brown curves). Trends (year<sup>-1</sup>) are plotted when significant according to the Student t-test, as summarized in Table 3.

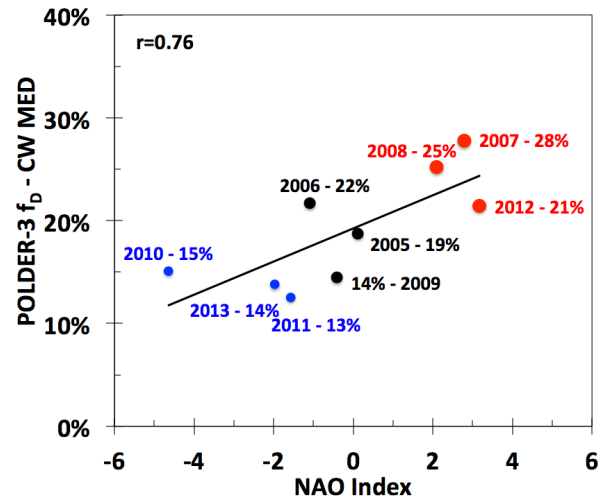
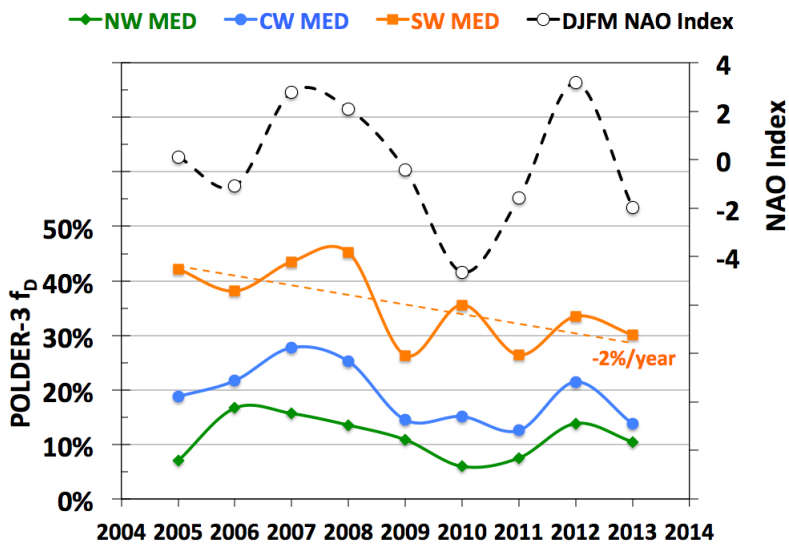


**Figure 10.** Left: Time series of the NAO winter Index (scale on the right axis, open circles) and of the following annual relative frequency ( $f_D$ ) of POLDER-3 AOD<sub>c</sub> at 865 nm  $\geq 0.10$  for the three sub-regions (NW MED in green, CW MED in blue, SW MED in orange) over the period March-2005–October 2013. The only significant trend of  $f_D$ /year is reported on the graph for SW MED. Right: Scatterplot of  $f_D$  versus preceding winter NAO Index for the CW MED region.



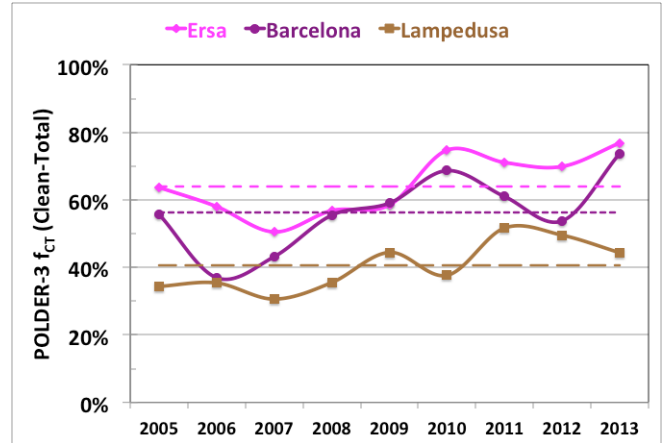
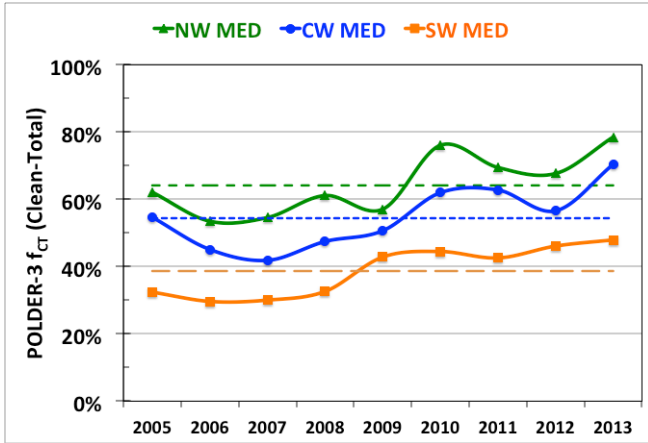
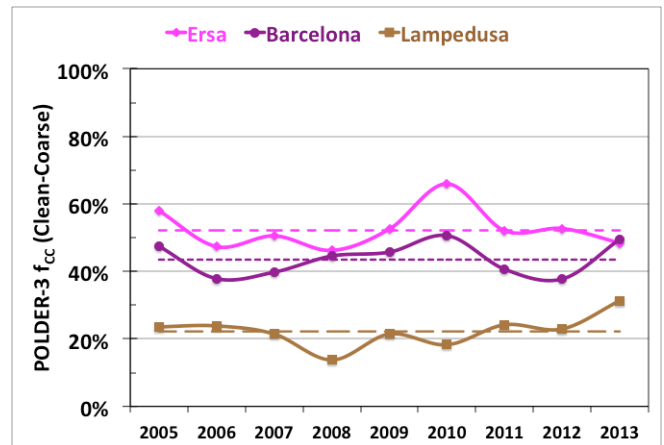
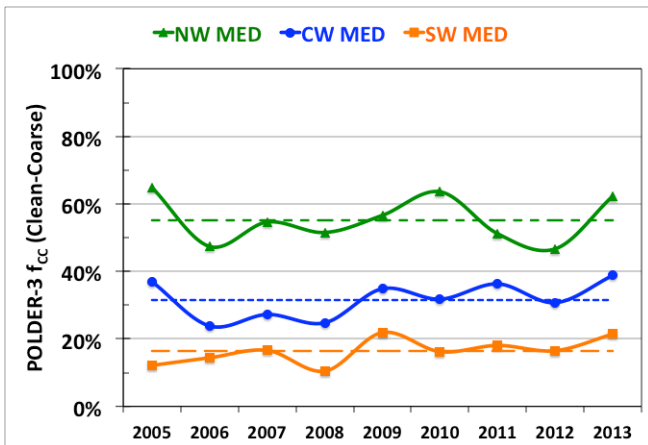
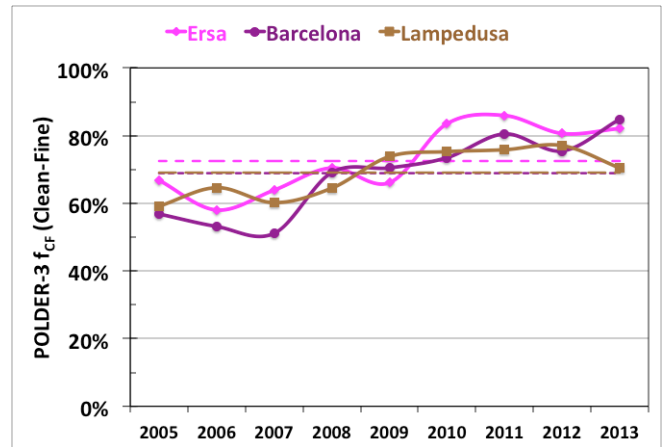
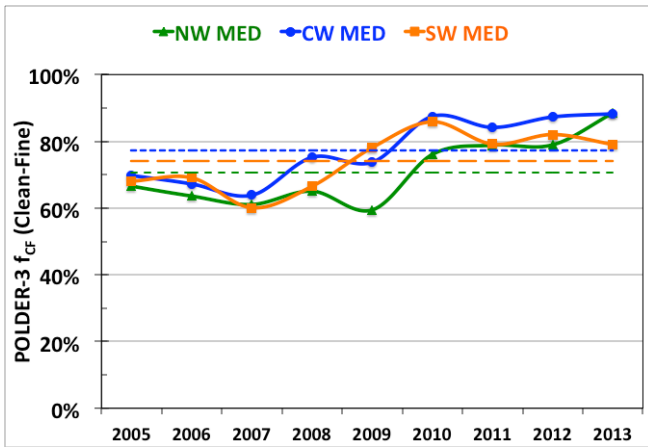


**Figure 11.** Left: Time series of annual (March–October) relative frequencies of occurrence of clean conditions for fine mode aerosol component (POLDER-3  $AOD_F$  865 nm below 0.05,  $f_{CF}$ ; top panel), coarse mode aerosol component (POLDER-3  $AOD_C$  865 nm below 0.05,  $f_{CC}$ ; middle panel), and total aerosol (POLDER-3  $AOD$  865 nm lower or equal to 0.10,  $f_{CT}$ ; bottom panel) over the period 2005–2013 for the three sub-regions NW MED, CW MED, SW MED. The dashed lines indicate the multi-year annual averages of relative frequencies. Right: Same for the three sites of Ersá, Barcelona, and Lampedusa.

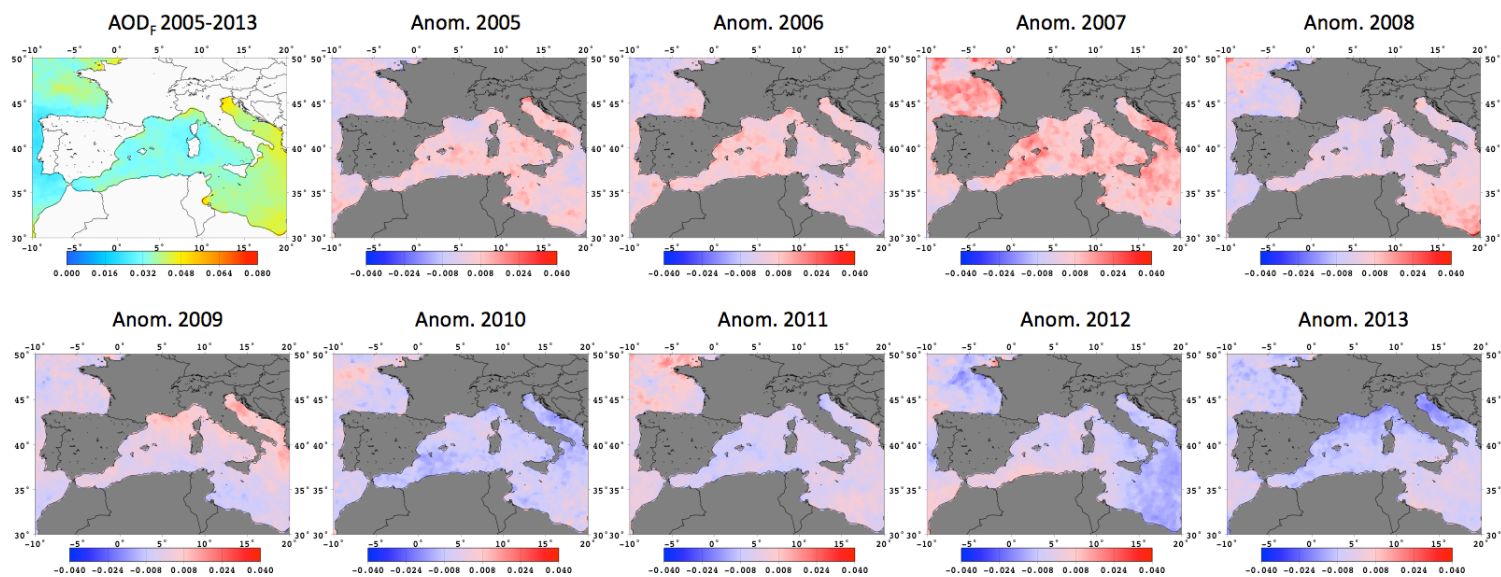


**Figure 12.** POLDER-3 AOD<sub>F</sub> at 865 nm averaged over the March-October period and the 9 years 2005-2013 (top left) and associated AOD<sub>F</sub> anomalies for each year.

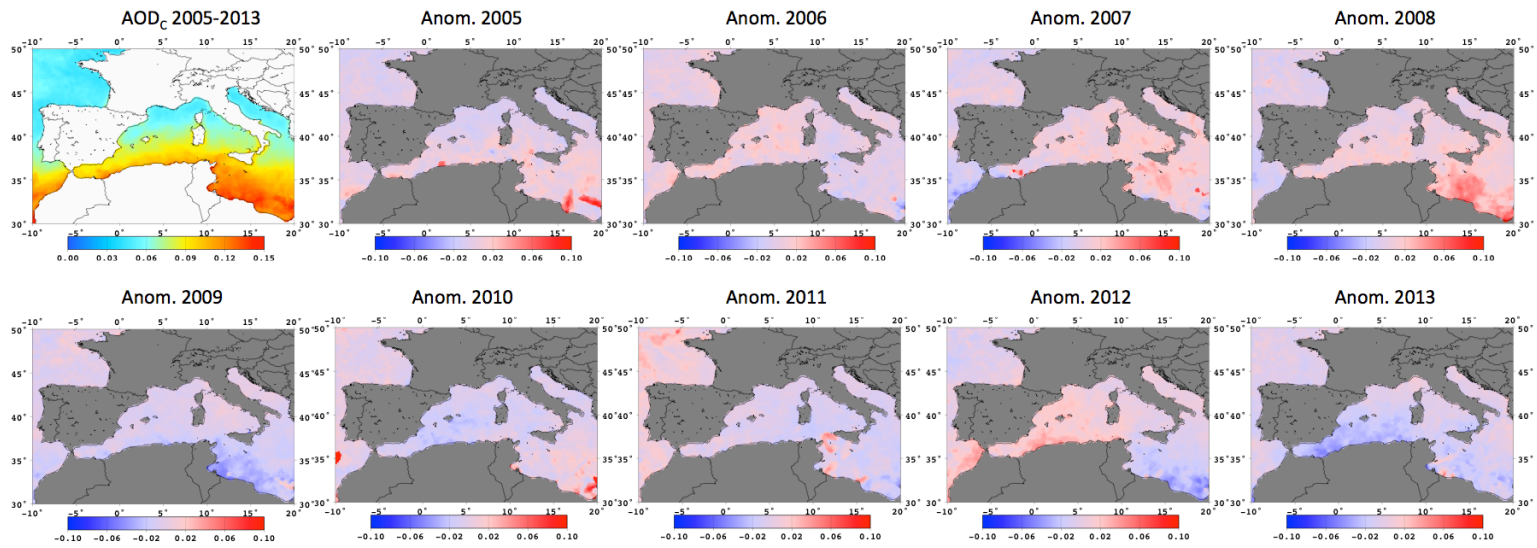


**Figure 13.** POLDER-3 AOD<sub>c</sub> at 865 nm averaged over the March-October period and the 9 years 2005-2013 (top left) and associated AOD<sub>c</sub> anomalies for each year.